A titin missense variant drives atrial electrical remodeling and is associated with atrial fibrillation

Mahmud Arif Pavel,[1*#] Hanna Chen,[1*] Michael Hill,[1*] Arvind Sridhar,[1] Miles Barney,[1] Jaime DeSantiago,[1] Abhinaya Baskaran,[1] Asia Owais,[1] Shashank Sandu,[1] Faisal A. Darbar,[1] Aylin Ornelas-Loredo,[1] Bahaa Al-Azzam,[1] Brandon Chalazan,[4,5] Jalees Rehman,[1,3] Dawood Darbar[1,2,6#]

*Contributed equally to this work.

Affiliation:

[1]Division of Cardiology, Department of Medicine, [2]Department of Pharmacology, [3]Department of Biochemistry and Molecular Genetics, University of Illinois at Chicago, Chicago, IL, USA, [4]Division of Genetics, Genomics, and Metabolism, Department of Pediatrics, Lurie Children's Hospital of Chicago, Chicago, IL, USA [5]Department of Pharmacology, Northwestern University, Chicago, IL, USA, [6]Jesse Brown Veterans Administration Medical Center, Chicago, IL, USA.

Address correspondence to: [#] Mahmud Arif Pavel, Department of Medicine, University of Illinois at Chicago, Chicago, IL, 60612, USA. Email: gmmahmud@uic.edu [#] Dawood Darbar, Department of Medicine, University of Illinois at Chicago, Chicago, IL, 60612, USA. Email: darbar@uic.edu

ABSTRACT

Rare and common genetic variants contribute to the risk of atrial fibrillation (AF). Although ion channels were among the first AF candidate genes identified, rare loss-of-function variants in structural genes, such as *TTN*, have also been implicated in AF pathogenesis, partly through the development of atrial myopathy; however, the underlying mechanisms are poorly understood. While *TTN* truncating variants (*TTN*tvs) have been causally linked to arrhythmia and cardiomyopathy syndromes, the role of missense variants (mvs) remains unclear. We show that rare *TTNmvs* are associated with worse clinical outcomes in a single-center ethnic minority clinical cohort and uncover a pathogenic mechanism by which the T32756I variant drives AF. Modeling the *TTN*-T32756I variant using human induced pluripotent stem cell-derived atrial cardiomyocytes (iPSC-aCMs) revealed that the mutant cells display aberrant contractility, increased activity of a cardiac potassium channel (KCNQ1, Kv7.1), and dysregulated calcium homeostasis without compromising the sarcomeric integrity of the atrial cardiomyocytes. We also show that a titin-binding protein, the Four-and-a-Half Lim domains 2 (FHL2), has increased binding with KCNQ1 and its modulatory subunit KCNE1 in the *TTN*-T32756I-iPSC-aCMs, enhancing the slow delayed rectifier potassium current (I_{ks}). Suppression of FHL2 in mutant iPSC-aCMs normalized the I_{ks}, supporting FHL2 as an I_{ks} modulator. Our findings demonstrate that a single amino acid substitution in titin not only impairs its function but also remodels ion channels, contributing to AF. These findings underscore the importance of high-throughput screening to assess the pathogenicity of *TTN*mvs and establish a mechanistic

connection between titin, potassium ion channels, and sarcomeric proteins, which may represent a novel therapeutic target.

INTRODUCTION

Atrial fibrillation (AF), the most prevalent cardiac arrhythmia, affects more than 60 million people worldwide and is associated with increased risk for stroke, heart failure, and dementia, justifying it as a major public healthcare burden[1,2]. AF is characterized by irregular and often abnormally fast heart rates[3,4]. Over the last decade, tremendous progress has been made in understanding the genetic architecture of AF[5–7]. Genome-wide association studies have identified over 140 common loci associated with AF, while family-based studies have implicated rare variants primarily encoding ion channels[8,9]. Although AF has been traditionally classified as a 'channelopathy', variants in myocardial sarcomeric proteins such as titin have been increasingly associated with familial or early-onset AF[10,11].

The *TTN* gene encodes for a massive myofilament (~4200 kDa), titin, which stretches along the Z-disk (N-terminus) to the M-band (C-terminus) region of the sarcomere[12,13]. Titin serves as a molecular scaffold for other muscle proteins, participates in downstream signaling, and provides passive tension in cardiac muscle[14,15]. Due to its large size, the rate of genetic variation in *TTN* is high, including both truncating (*TTN*tvs) and missense variants (*TTN*mvs)[16,17]. The prevalence of rare *TTN*tvs and *TTN*mvs in the general population is 2% and 5.7%, respectively[18–20]. While *TTN*tvs are the most common genetic cause (10-20%) of dilated cardiomyopathy (DCM), *TTN*mvs are often disregarded in clinical practice, and are considered benign in DCM-specific variant interpretation frameworks based on the American College of Medical Genetics (ACMG) recommendations[21,22]. Yet, *TTN*mvs may have the potential to confer disease, as a

recent study in two families revealed that *TTN*mvs in a conserved cysteine of *TTN* can cause DCM[23]. Another study demonstrated segregation of a novel *TTN*mv in five individuals with atrioventricular block in a Chinese family, suggesting that *TTN*mvs may also be implicated in arrhythmia syndromes[24]. To date, a relationship between rare *TTN*mvs and AF has not been explored at either clinical or mechanistic levels. This has potentially heightened importance across racial and ethnic groups, in whom the likelihood of detecting variants of uncertain significance (which are predominantly *TTN*mvs) is higher than in individuals of European descent[25].

Despite the clinical importance, the pharmacological therapy of AF is limited in part because of the incomplete understanding of the myocardial substrate for AF, as human atrial tissue is rarely available, and the limitations of existing in vitro and in vivo models[26]. However, human induced pluripotent stem cell-derived atrial cardiomyocytes (iPSC-CMs) not only possess the complex array of cardiac ion channels that make up the atrial action potential (AP) but also hold great promise for modeling AF[27,28]. Modeling patient-specific mutations associated with familial AF using mature human iPSC-CMs offers a powerful, naturally integrated system with distinct advantages over animal models and heterologous expression systems[29]. Recent reports using human iPSC-CM models have elucidated the pathophysiological mechanisms of DCM[30], hypertrophic cardiomyopathy[31], Brugada syndrome[32], long QT syndrome[33], and AF[27,29,34]. Human iPSC-CMs also have the potential to uncover the molecular mechanisms of AF, as they can be easily modified to contain the precise genetic background of the individual patient[35–37].

To examine the potential role of *TTN*mvs in AF, we examined the prevalence of rare *TTN*mvs in a single-center cohort of African-American and Hispanic/Latinx individuals with AF who underwent whole exome sequencing, compared clinical characteristics between *TTN*mv carriers and non-carriers, and evaluated whether *TTN*mvs were associated with increased risk of AF or heart failure (HF)-related hospitalizations. To explore whether the *TTN*mvs may be mechanistically linked to the development of AF, we introduced a rare *TTN*mv (*TTN*-T32756I) into human iPSC-aCMs using clustered regularly interspaced short palindromic repeats-associated 9 (CRISPR-Cas9). We performed electrophysiological (EP), pharmacological, and mechanistic analyses to elucidate the mechanisms underlying *TTN*mv-induced AF. Our study demonstrated that *TTN*-T32756I iPSC-aCMs exhibited a striking AF-like EP phenotype in vitro. Transcriptomic analyses revealed that this *TTN*mv enhances the activity of the Four-and-a-half LIM domain protein 2 (FHL2), which, in turn, modulates the slow delayed rectifier potassium current (I_{Ks}), thereby promoting AF susceptibility.

RESULTS

***TTN*mvs are associated with increased hospitalization risk in a multiethnic cohort with AF.** *Clinical characteristics:* A total of 131 subjects were included (mean [SD] age at AF diagnosis 63.5 [13.8] years, 70 [53.4%] male, 38 [29%] Hispanic/Latinx, 93 [71%] non-Hispanic Black; **Table 1**). We identified 138 *TTN*mvs, most commonly in the *TTN* A-band (108 [78.8]%), followed by the I-band (20 [14.6%]), M-band (2 [1.5%]), near the Z-disk (6 [4.4%], and in the Z-disk (2 [1.5%]) (**Figure 1A, Supplementary Table 1**). Based on the REVEL *in silico* score, 52 (37.7%) *TTN*mvs variants were predicted to be deleterious. A total of 77 (58.8%) subjects carried a *TTN*mv, with 43 (32.8%) carrying a

predicted deleterious variant. Carriers of a *TTN*mv had a higher QTc interval on electrocardiogram (ECG) closest to AF diagnosis (mean [SD] 466.5 [42.3] vs. 449.6 [37.7] ms, P=0.027); there were otherwise no other significant clinical or demographic differences between variant carriers and non-carriers. When stratifying by predicted deleterious *TTN*mv only (**Supplementary Table 2**), a higher proportion of variant carriers were non-Hispanic Black (36 [83.7%] vs. 57 [64.8%], P=0.026). On index ECG, carriers additionally had higher ventricular rate (mean [SD] 103.7 [31.4] vs. 90.9 [27.4] beats/min, P=0.022), QTc interval (mean [SD] 470.6 [44.0] vs. 453.9 [38.7] ms, P=0.035), and LVEDD on index echocardiogram (mean [SD] 49.8 [8.0] vs. 45.6 [9.2] mm, P=0.021). Seventeen (15.2%) subjects met criteria for left ventricular (LV) dilatation, with a higher proportion of LV dilatation in *TTN*mv carriers but without a significant difference compared to non-carriers (13 [20.3%] vs. 4 [8.3%], P=0.111). Twelve subjects (9.2%) met criteria for a clinical diagnosis of nonischemic DCM based on a left ventricular ejection fraction (LVEF) <50%, presence of LV dilatation, and confirmation of non-severe coronary artery disease by coronary angiography. Of those, 8 subjects carried *TTN*mvs of which 6 were predicted to be deleterious (**Supplementary Table 3**).

*TTN*mvs *are associated with higher hospitalization risk:* A total of 174 hospitalizations (64 AF-related and 110 HF-related) occurred after a median (interquartile range [IQR]) follow-up time of 4.14 (1.25-6.04) years, with 119 (68.4%) events occurring in *TTN*mv carriers and 55 (31.6%) of events occurring in non-*TTN*mv carriers. Thirty-nine (50.6%) subjects with a *TTN*mv experienced at least one hospitalization during the follow-up

period compared to 22 (40.1%) of non-carriers, and total hospitalization incidence rate was 32.2 events per 100 person-years (p-y) in *TTN*mv carriers compared to 17.4 per 100 p-y in non-carriers. Mean cumulative incidence is shown in **Figure 1B**. The unadjusted hazard of hospitalization by 10 years was significantly higher in *TTN*mv carriers compared to noncarriers (hazard ratio [HR] 1.81, 95% confidence interval [CI] 1.04-3.15, p=0.036). This remained significant after partial adjustment for age and sex (HR 1.82, 95% CI 1.04-3.17, p=0.035) as well as full adjustment that additionally included ethnicity and baseline LVEF <50% (HR 1.80, 95% CI 1.03-3.15, p=0.039; **Supplementary Table 4**). No other covariates were significantly associated with the outcome. To assess whether baseline LVEF influenced the relationship between *TTN*mvs and hospitalization risk, an interaction term between LVEF<50% and the presence of *TTN*mvs was tested and was not significant (interaction P=0.843). To assess whether the prediction of deleterious effect influenced the relationship between *TTN*mv presence and hospitalization risk, subgroups based on high or low REVEL score were separately examined (**Supplementary Table 5**). Compared to non-*TTN*mv carriers, hospitalization risk was significantly increased in subjects carrying predicted deleterious *TTN*mvs (HR 1.92, 1.04-3.53, P=0.036). While subjects with *TTN*mvs not expected to be deleterious also had an elevated point estimate of hospitalization risk, this difference was not significant (HR 1.60, 95% CI 0.78-3.28, P=0.198). Findings remained similar with the exclusion of patients with nonischemic DCM (**Supplementary Table 6**). While in a previous study we identified likely pathogenic or pathogenic AF variants in 7.0% of ethnic minority probands, with most (46.7%) *TTN*tvs[11], these results suggest that *TTN*mvs are also linked with adverse clinical outcomes, and missense

variants should be considered in assessing pathogenicity in clinical and genetic contexts.

A single amino acid change in a *TTN*mv is potentially causative of AF. We identified three early-onset paroxysmal AF probands from separate families harboring the same rare *TTN*mv (Chr 2q31.2 (GRCh38): g. 178539797G>A) without additional loss-of-function *TTN* variants. The clinical characteristics of the three probands are summarized in **Table 2**. This missense variant localizes in the A-band of *TTN* and causes the substitution of a conserved residue threonine by an isoleucine (p.Thr32756Ile, NM_001267550.2 (TTN), c.98267C>T (**Figure 1C-D, Supplementary Figure 1A**). In the gnomAD reference population, the *TTN*-T32756I variant has a frequency of 0.000245 overall, 0.0046 within the subpopulation of African ancestry, and is impartially distributed across sexes and ages (**Figure 1E, Supplementary Figure 1B-E**). The *TTN*mv has also been described in Clinvar (NM_001267550.2(TTN):c.98267C>T (p.Thr32756Ile), **Supplementary Table 7**) and gnomAD v4.0.0 (SNV:2-178539798-G-A(GRCh38)) in patients with DCM and other diseases.

***TTN*-T32756I iPSC-aCMs exhibit aberrant contractility without compromising sarcomere integrity.** To functionally characterize the *TTN*-T32756I variant, we exploited wild-type (WT) human iPSC lines and introduced the point mutation c.98267C>T in the *TTN* allele (**Figure 2A, Supplementary Figure 2A-B**). The iPSC lines expressing the pluripotent markers Sox2 and Oct4 and showing normal karyotype were first differentiated into cardiomyocytes (**Supplementary Figure 2C-D**), and then a

retinoic acid-based and comprehensive maturation protocol was applied to generate the iPSC-aCMs as we described previously[26,27]. Given that cardiac contractility is a key component of heart function and is linked to cardiac disorders associated with *TTN*[38], we first assessed the contractility of the WT and mutant iPSC-aCMs and observed both reduced contraction duration and abnormal relaxation in *TTN*-T32756I-iPSC-aCMs (**Figure 2B-E, Supplementary Figure 3A-B**). Compared to WT, the beating frequency of the *TTN*-T32756I-iPSC-aCMs was significantly increased (52 ± 7.8 vs. 98 ± 7.5 beats per min, P=0.001; **Figure 2C**) coupled with the reduction of the contraction duration (456.5 ± 61.45 vs 262.9 ± 48.16 msec, P=0.032; **Figure 2D**), the peak-to-peak time (1529 ± 195.5 vs 636.6 ± 135.8 msec, P=0.004; **Supplementary Figure 3B**), and the relaxation duration (281.5 ± 42.95 vs 79.40 ± 21.14 msec, P=0.003; **Supplementary Figure 3A**). In contrast, the contraction amplitude of the mutant was increased (8.1 ± 0.8 vs 10.6 ± 7 au, P=0.040) without any significant changes in time-to-peak (**Figure 2E, Supplementary Figure 3C**), suggesting an increased contractile force by the *TTN*-T32756I-iPSC-aCMs. As sarcomere disorganization is often observed in *TTN*-related cardiomyopathies and underlies contractile dysfunction[39], we explored whether *TTN*mvs perturbed the organization of the sarcomere. Surprisingly, we did not find any disarray in the sarcomeres of either WT or *TTN*-32756I-iPSC-aCMs. Using transmission electron microscopy (TEM) and immunofluorescence (IF), we observed symmetrical arrays of recurring sarcomeres in the WT and the mutant atrial cardiomyocytes with no changes in the sarcomere length (**Figure 2F-G, Supplementary Figure 3D-F**). Although no sarcomeric perturbation by the T32756I variant was observed, the aberrant contractility

displayed by the *TTN*-T32756I-iPSC-aCMs suggests that the *TTN*mv may be pathogenic.

Altered cardiac potassium current and calcium handling underlie the arrhythmia phenotype in *TTN*-T32756I-iPSC-aCMs. As studies have shown that abnormal atrial electrophysiology and calcium-handling underlie atrial arrhythmogenesis and contractile dysfunction[40,41], we hypothesized that the *TTN*-T32756I variant modulates atrial APs, ion channels and intracellular calcium. We first tested the spontaneous and paced AP characteristics of the isolated WT and the *TTN*-T32756I iPSC-aCMs, which revealed a significant shortening of the AP duration (APD) at 10%, 50%, and 90% repolarization; however, there was no change in the peak amplitude (**Figure 3A-C, Supplementary Figure 4A-B**). Since increased potassium current (I_k), especially the augmented delayed rectifier potassium current (I_{ks}), causes AF by reducing the APD[27,42], we assessed I_{ks} by using whole-cell voltage clamping. We observed an increase in both I_k and I_{ks} in *TTN*-T32756I-iPSC-aCMs compared with the WT (**Figure 3D-F, Supplementary Figure 4C-E, Supplementary Figure 5A-D**); thus, confirming that the APD shortening is partly due to the increased I_k. To test the effect of T32756I on atrial calcium handling, we measured the intracellular calcium transients at the excitation-contraction coupling moment of the iPSC-aCMs using fluorescent calcium imaging. Compared to WT, spontaneously beating *TTN*-T32756I-iPSC-aCMs exhibited increased frequency along with a significant reduction in the time to 50% and 90% decline of calcium transients (**Figure 3G-I, Supplementary Figure 4F**). We also saw a similar decile of calcium transients in the paced iPSC-aCMs (**Supplementary Figure 5E-H**).

However, *TTN*-T32756I-iPSC-CMs exhibited similar calcium transient amplitudes as the WT, indicating that there was no change in the availability of the intracellular calcium for each contraction (**Supplementary Figure 4G, Supplementary Figure 5**). Our findings suggest that the reduced APD resulting from increased potassium current and the altered timing of the calcium transient may create a reentrant substrate for AF.

RNA sequencing analysis reveals alterations in cardiac signaling and disease pathways in *TTN*-T32756I-iPSC-aCMs. To elucidate the underlying molecular mechanism by which *TTN*-T32756I is associated with contractile defects and ion channel remodeling, we performed transcriptomic sequencing of mutant iPSC-aCMs and WT. Comparison of total RNA levels in *TTN*-T32756-iPSC-aCMs with WT-iPSC-aCMs and differential expression analysis showed genes related to cardiac muscle contraction and calcium handling were predominantly affected (**Figure 4A, Supplementary Figure 6A-C**). Gene-ontology (GO) pathway enrichment further showed that the top significantly downregulated cardiac-related GO Biological Processes (-BP) in *TTN*-T32756I iPSC-aCMs included key processes such as cardiac myofibril assembly, skeletal muscle myosin thick filament assembly, extracellular matrix organization, and regulation of potassium ion transmembrane transporter assembly among others (**Figure 4B**). As for GO-Molecular function pathways (GO-MF), outward potassium channel activity, voltage-gated potassium channel activity, calcium channel activity, and gap junction channel activity were enriched (**Figure 4C**). Kyoto Encyclopedia of Genes and Genomes (KEGG) pathway analysis identified downregulation in critical pathways including Adrenergic signaling in cardiomyocytes,

the Phosphoinositide 3-kinase (PI3K) signaling pathway, Dilated cardiomyopathy pathway, Hypertrophic cardiomyopathy pathway and Calcium signaling pathway (**Figure 4D**), which are crucial for normal cardiac electrophysiology and contractility. Upregulated pathways in both GO and KEGG analyses were mostly restricted to neuronal pathways, including axon and neuron development, the Hippo signaling pathway, and the Notch signaling pathway. In the transcriptomic analysis of *TTN*-T32756I-iPSC-aCMs, several transcription factors (TFs) showed significant alterations, highlighting their potential roles in the mutation's impact (**Figure 4E, Supplementary Figure 6D**). Top-cardiac related upregulated TFs include *MYC*, linked to cell growth and apoptosis, suggesting an increase in cellular proliferation. Stress-related TFs such as *NFE2L2* and *CEBPB* are also elevated, indicating a heightened stress response. Additionally, TFs like *ESRRA* and *FOXM1*, which regulate metabolic processes and cell cycle, respectively, and *FOXO1* which regulates metabolism and stress resistance. Key TFs in muscle function, such as MYOD1, MYOCD, KLF5, and NKX2.5, were enhanced, alongside *SMAD2*, *CREBBP*, *PITX2*, *NFKB1*, and *GATA4*, which are vital for diverse roles ranging from signal transduction to immune regulation (**Figure 4E**). Conversely, downregulated transcription factors include *SIRT1*, which plays a role in cellular stress resistance and mitochondrial function, pointing to potential vulnerabilities in cellular defenses. Cardiovascular-related TFs such as *KLF2* and *KLF3*, along with *SMAD7*, involved in TGF-beta signaling, were reduced, possibly impacting structural and signaling integrity. Additionally, *MXD1* and *IKZF1*, crucial for cellular differentiation and immune development, were also diminished (**Figure 4E**). These transcriptional changes

underscore a complex network of regulatory adjustments that could contribute to the altered EP and structural properties in *TTN*-T32756I-iPSC-aCMs.

Using the KEGG and GO pathways, we performed Ingenuity Pathway Analysis (IPA) to identify novel titin-interacting proteins that could account for the increased I_{ks} activity in *TTN*-T32756I-iPSC-aCMs. The IPA suggests FHL2, which is known to transduce mechanical signaling through its interactions with titin and is enriched in the mutant iPSC-aCMs (**Figure 4F**). As FHL2 has also been shown to interact with the I_{ks}-binding partner mink (KCNE1) directly and increases its current density[43], we postulate that elevated FHL2 levels in *TTN*-T32756I-iPSC-aCMs may enhance binding to I_{ks} and thus increase its activity.

The FHL2 mediates the enhanced I_{ks} current in *TTN*-T32756I-iPSC-aCMs. To determine if *TTN*-T32756I increases I_{ks} by modulating the interaction between KCNQ1-KCNE1 and FHL2, we performed co-immunoprecipitation studies and confocal microscopy in both WT and *TTN*-T32756I-iPSC-aCMs. The co-localization between KCNE1 and FHL2 increased ~3-fold in *TTN*-T32756I-iPSC-aCMs, suggesting an increased interaction between them (**Figure 5A, Supplementary Figure 7**). Since FHL2 enhances I_{ks} activity, we investigated whether inhibiting FHL2 could reverse the increased I_{ks} observed in the *TTN*-T32756I-iPSC-aCMs. To inhibit FHL2, we employed small interfering (si) RNA to suppress *FHL2* expression and measured I_{ks} activity in both WT and *TTN*-T32756I-iPSC-aCMs. Both the WT and mutant iPSC-aCMs transfected with FHL2-specific siRNA showed a substantial decrease in FHL2 expression (**Figure**

5B). As shown in **Figure 5C-D**, voltage-clamp recordings demonstrate that the I_{ks} in FHL2-suppressed *TTN*-T32756I-iPSC-aCMs are significantly reduced compared to the corresponding I_{ks} in *TTN*-T32756I-iPSC-aCMs but comparable to the WT (**Figure 5D)**. Therefore, inhibition of FHL2 by the siRNA rescues the increased I_{ks} of the *TTN*-T32756I-iPSC-aCMs, which is similar to that of WT I_{ks}. Overall, our data suggest that the *TTN*mv creates an EP substrate for AF by modulating I_{Ks} activity, in part by increasing the interaction between the KCNQ1-KCNE1 complex and FHL2 (**Figure 5E)**.

DISCUSSION

We identified an association between *TTN*mvs and adverse clinical outcomes in a multiethnic cohort of patients with AF and elucidated a causal mechanism by which a *TTN*mv can drive atrial remodeling and promote AF development. Although *TTN*tvs are a well-recognized cause of DCM and have been associated with early-onset AF[10,44], the role of *TTN*mvs in the pathogenesis of either arrhythmia or cardiomyopathy is unknown. Here, we demonstrate that rare, deleterious *TTN*mvs are associated with an elevated risk of hospitalization in a multiethnic cohort of patients with AF and show that a *TTN*mv can promote AF by impairing contractility and remodeling ion channels in atrial cardiomyocytes. Furthermore, we demonstrate that augmented I_{Ks} activity mediated by FHL2 can create a substrate for AF. Together, these findings establish a mechanistic role for *TTN*mvs in AF pathogenesis and highlight I_{Ks} and FHL2 as potential therapeutic targets for TTN-related arrhythmias.

The genetic architecture of AF is complex, with both monogenic and polygenic contributions that intersect with age and comorbidities to define an individual's risk. Despite AF being traditionally considered an ion channelopathy, the sarcomeric gene, *TTN,* is the most common in which rare loss-of-function variants have been associated with AF[10,45], and the penetrance of such variants was found to be even greater for AF than for HF in the UK Biobank[46]. As rare *TTN* variants comprise the strongest monogenic contribution to AF risk, we sought to explore whether *TTN*mvs may similarly affect AF development or outcomes. A study of 147 probands with DCM identified 44 severe *TTN*mvs in 37 probands, which clustered in the A-band region[17]. There were no differences in heart transplant-free survival between carriers and noncarriers. In a more recent study of 530 subjects with DCM using more stringent allele-frequency criteria, 31 predicted deleterious variants were identified, also predominantly located in the A-band[19]. However, these *TTN*mvs were found at similar frequencies to reference populations. Finally, a study of two families with DCM demonstrated segregation of *TTN*mvs affecting the same highly conserved cysteine residue in the I-band, which showed impaired contraction and folding at physiological temperatures in a homozygous iPSC model, demonstrating that a *TTN*mv can cause DCM[23].

We identified *TTN*mvs in 58% of subjects in our cohort, and 33% carried a potentially deleterious variant, as predicted by REVEL *in silico*. This frequency was higher than the 37/147 (25.2%) of *TTN*mv carriers in a DCM cohort[17], understanding that differing methods of bioinformatic filtering may limit the ability for direct comparison. Consistent with prior studies, most deleterious variants in our study were found in the A-band[47,48],

where *TTN*tvs have been most strongly linked to disease. The presence of predicted deleterious *TTN*mvs was associated with a higher LV end-diastolic diameter, but without a statistically significant difference in LVEF, potentially suggesting overlap between subclinical left ventricular cardiomyopathy and AF in these subjects. Notably, rates of baseline heart failure diagnosis (encompassing both reduced and preserved ejection fraction) were similar based on *TTN*mv carrier status. We also noted higher ventricular rate and QTc interval on index ECGs in these subjects. Rare deleterious variants in *TTN* have previously been associated with changes in the QT interval[49], but the mechanism for this remains unclear. Finally, evidence on the relationship between *TTN*mvs and clinical outcomes is sparse, with only a few studies examining event-free survival in DCM patients. We observed a significant association between *TTN*mv presence and increased cumulative incidence of AF or HF-related hospitalizations, which remained unchanged in multivariable adjustment and in sensitivity analyses. This importantly suggests that *TTN*mvs may correlate with disease severity. Our cohort is derived from a single-center multi-ethnic registry of individuals with AF. It lacks a matched cohort of non-AF controls to compare the incidence of *TTN*mvs. Further study exploring these associations in multi-ethnic, larger validation cohorts that include both AF and non-AF individuals,and examining AF-specific measures such as arrhythmia burden or treatment response, will be necessary to fully understand the clinical importance of *TTN*mvs in AF.

Prediction of missense variant impact using *in silico* tools and algorithms can be limited by low specificity, contributing to challenges in clinical interpretation[50]. Functional

367 studies are often helpful in these cases to confirm or support variant pathogenicity. As
368 existing in vitro or in vivo models do not adequately replicate the complexity of AF,
369 human iPSC-aCMs possess the complex array of cardiac ion channels that make up the
370 atrial AP and provide an adequate model to establish causal relationships in AF[26]. We
371 identified the missense variant *TTN*-T32756I in three unrelated subjects in our
372 multiethnic AF registry. Hypertension is a common comorbidity in patients with AF and
373 could contribute to disease progression. However, all three individuals carrying *TTN*-
374 T32756I exhibited early-onset AF (onset before 66 years). This suggests a two-hit
375 mechanism, in which genetic predisposition and comorbidities influence disease risk.
376 Importantly, our iPSC model isolates the genetic effects of *TTN*-T32756I from other
377 factors, supporting a direct pathogenic role. Remarkably, a single amino acid change in
378 the giant protein titin results in aberrant contractility and EP remodeling without affecting
379 sarcomeric integrity. Although we did not observe any defects in the sarcomere, in a
380 separate study, including T32756I in the same area, caused significant perturbation in
381 sarcomere assembly[37]. T32756 corresponds to a conserved Threonine of the Ig139
382 domain (UniProt# Q8WZ42, predicted Ig155 by TITINdb2), and the replacement of a
383 conserved hydrophilic residue (Thr) in WT with a hydrophobic residue (Ile) may cause
384 thermal instability and destabilize the domain. It is now well recognized that point
385 mutations may drastically disrupt the Ig domains and could unfold under pathological
386 conditions[51]. Such mutations have been proposed to modify titin-based passive stiffness
387 and may lead to cardiomyopathy. Missense mutations such as T2850I, R57C, and
388 S22P in the I-band titin have been reported to significantly destabilize Ig domains and
389 display a higher tendency to unfold[52,53]. Likewise, T32756I may unfold under the

physiological settings and increase susceptibility to protein loss (haploinsufficiency) or degradation (poison peptide effect), leading to impaired sarcomere function. Furthermore, as titin acts as a crucial signaling hub that transduces mechanical forces to downstream signaling pathways within cardiomyocytes and interacts with various sarcomeric proteins and signaling molecules[13,54], subtle destabilization of Ig139 domain by the T32756I could alter the biochemical signals that regulate various downstream signaling pathways involved in cardiac function and adaptation. Hence, the contractile and ion channel dysfunction caused solely by homozygosity for T32756I in iPSC-aCMs suggests that the *TTN*-T32756I missense variant can drive atrial remodeling. While our CRISPR-edited isogenic *TTN*-T32756I iPSC-aCMs provide genetically controlled for minimizing the genetic background variability and dissecting variant-specific effects, future studies using multiple iPSC backgrounds and patient-derived lines will be critical for confirming the robustness and generalizability of the observed phenotypes.

Although several studies have identified possible pathways associated with *TTN*tvs and AF, the pathogenic mechanisms of *TTN*mv-associated AF remain unclear. We show for the first time that the T32756I creates an EP substrate for AF by ion channel remodeling with an enhanced I_{Ks}, which is mediated by a titin-interacting protein FHL2. FHL2 is enriched in cardiac muscle and is a multifunctional protein that regulates cardiac myocyte signaling and function[55]. FHL2 interacts with KCNE1, which binds to the outer face of the KCNQ1 channel pore domain and may modify the interactions between the voltage sensor, S4-S5 linker, and the pore domain to augment the channel current[43]. It has been suggested that FHL2 interacts with the titin N2B segment, titin kinase domain,

and forms a complex with other proteins, such as MURF1 and MURF2, calmodulin, and Nbr1, playing a role in hypertrophy signaling and the atrophy response[56,57]. It also binds to the edge of titin (M-line), which is in close proximity to T32756I, and interacts with myospryn and obscurin[58]. It is tempting to postulate that T32756I may interfere with FHL2's interaction with titin, thereby disrupting subsequent mechano-biochemical signaling and increasing FHL2's availability for binding to the KCNQ1-KCNE1 complex. While our study provides mechanistic insights into the role of the *TTN*-32756I missense variant in AF, *TTN*mvs may modulate ion channels and regulate atrial rhythmicity through multiple interrelated signaling pathways. Further studies are needed to fully uncover the molecular basis of this regulation and its implications for AF pathophysiology and potential therapeutic interventions.

In summary, this study demonstrates an association between *TTN*mvs and AF, suggesting that *TTN*mvs may contribute to adverse clinical outcomes in patients with AF and establishing a mechanism by which a particular *TTN*mv may influence AF development. We identify a critical role for FHL2 in modulating the atrial action potential by interacting with the Kv7.1–KCNE1 complex, thereby enhancing I_{Ks} in *TTN*-T32756I iPSC-aCMs. Importantly, suppression of FHL2 rescued the augmented I_{Ks}, indicating that targeting FHL2 or I_{Ks} may help restore sinus rhythm and improve atrial contractility. These findings provide mechanistic insight into how *TTN*mvs can promote arrhythmogenesis and highlight KCNQ1 and FHL2 as potential therapeutic targets for TTN-related AF. Further studies are warranted to validate this mechanism and to determine whether *TTN*mvs in other titin domains induce AF through similar pathways.

Although the effects of *TTN*-T32756I in iPSC-derived ventricular cardiomyocytes remain to be explored, future work may clarify whether this variant produces comparable or distinct EP alterations. Collectively, our findings broaden the understanding of *TTN*-related atrial pathophysiology, underscore the importance of incorporating *TTN*mvs into genomic analyses of AF, and emphasize the value of functional validation in advancing precision medicine for patients carrying rare sarcomeric variants.

METHODS

Study population

The UIC Multi-Ethnic AF Biorepository was established in 2015 to explore the genetic basis of AF across racial and ethnic groups. This study was approved by the UIC Institutional Review Board (#2015-0681). Subjects are prospectively enrolled from outpatient and inpatient sites within the University of Illinois Health (UIH) healthcare system. Subjects must have a documented history of AF by electrocardiogram, Holter/event monitor, or implantable cardiac device, with confirmation by an attending cardiologist. At the time of enrollment, blood is drawn for DNA extraction and genetic analysis. Baseline demographics are obtained from provider notes in the electronic health record (EHR) and, as necessary, confirmed with the patient at the time of enrollment. Longitudinal clinical outcomes are followed through serial review of the EHR. Written informed consent was obtained from all participants. Adults 18 years of age or older at the time of AF diagnosis were prospectively enrolled between August 25, 2015, and May 19, 2019. Samples from 161 subjects who identified as non-Hispanic Black (NHB) or Hispanic/Latinx (HL) and had an echocardiogram performed within 3 months of enrollment date underwent whole exome sequencing. A total of 27 subjects with congenital or rheumatic disease, severe mitral stenosis, and end stage renal disease on dialysis were excluded. Three subjects who carried a predicted loss-of-function frameshift or stop-gain *TTN* variant were additionally excluded. The primary exposure was the presence of one or more missense *TTN* variants. The primary outcome was time from initial AF diagnosis to hospitalizations with a primary diagnosis of either AF or acute decompensated HF recorded in the clinical discharge summary,

captured as repeating events. Clinical data was obtained through manual review of EHR and comorbidities were defined if present in clinical notes on or prior to AF diagnosis date. Subjects were censored on date of death, last known clinical encounter (up to August 26, 2023), or at 10 years after AF diagnosis. Echocardiographic criteria for left ventricular dilatation was defined as left ventricular end diastolic diameter (LVEDD) > 2 standard deviations (SD) above sex-specific mean according to standard guidelines[59]. Subjects meeting echocardiographic criteria for left ventricular dilatation fulfilled clinical criteria for nonischemic dilated cardiomyopathy if left ventricular ejection fraction (LVEF) < 50% and ischemic cardiomyopathy was ruled out by coronary angiogram.

Whole exome sequencing

Samples were sequenced with support of the National Human Genome Research Institute (NHGRI) Centers for Common Disease Genetics (CCDG) program. Sequencing was performed at the Broad Institute following methods established by the National Heart, Lung, and Blood Institute (NHLBI) Trans-Omics for Precision Medicine (TOPMed) Atrial Fibrillation Study (available under TOPMed Whole Genome Sequencing Methods: Freeze 9 at https://www.ncbi.nlm.nih.gov/projects/gap/cgi-bin/study.cgi?study_id=phs001062.v5.p2). Samples underwent WES using an Illumina HiSeq X system with 150bp paired-end read length, at 20x depth for at least 85% of targets Alignment to human genome reference GRCh38/hg38 was performed using BWA-MEM (Burrows-Wheeler Aligner, v0.7.15.r1140). *TTN* variant calls were filtered to select those with read depth of ≥20X, genotype quality ≥20, minor allele frequency (MAF) ≤1% across gnomAD subpopulations, and excluding intronic, regulatory or UTR

3'/5' variants. Synonymous variants, homozygous reference calls, non-canonical variants, and any variants with percent spliced in (PSI) index <90 were excluded. Missense variants predicted to be deleterious were identified using REVEL score of ≥0.7, a previously proposed cutoff to predict deleterious effect in dilated cardiomyopathy[60,61]. Because of the uncertain role of missense *TTN* variants across AF and other cardiac diseases, we examined all *TTN* missense variants regardless of REVEL score. Variant annotation data were obtained from Ensembl Variant Effect Predictor[62], downloaded January 11, 2024, and CardioDB (https://cardiodb.org/titin) for *TTN* region and percent spliced in (PSI)[63], downloaded November 16, 2023. The TTN-T32756I variant (REVEL Score: 0.58758; Supplementary Table 1) was prioritized because it occurred in multiple unrelated individuals within our clinical AF cohort, despite no reported family history of AF in affected individuals. While no parental inheritance was observed, the possibility of de novo origin cannot be excluded. Furthermore, this variant is located within a region overlapping a deletion mutation recently shown to cause AF in a zebrafish model, supporting its potential pathogenicity[37]. Notably, the affected individuals did not carry additional loss-of-function TTN variants.

Human iPSC culture and human iPSC-aCM differentiation

Human iPSC-CMs were derived from reprogrammed peripheral blood mononuclear cells (PBMCs) as previously described[29]. 80-90% confluent iPSC-CMs were differentiated using the Cardiomyocyte Differentiation Kit (Gibco) and guided toward the atrial subtype using all-trans RA[64]. The cellular population was purified through glucose starvation and lactate replacement, resulting in contracting monolayers of iPSC-aCMs.

Our protocol typically yields ~80 to 90% pure iPSC-aCMs and <6% fibroblasts based on immunostaining analysis as we have previously described[29,64]. Human iPSC-aCMs were then matured following dissociation and replating on fibronectin-coated plates and maintained in Cardiomyocyte Maintenance Media supplemented with T3, insulin-like growth factor-1, and dexamethasone as previously described[27].

Generation of TTN-T32756I *hiPSCs using CRISPR-Cas9*

Due to the patients' unavailability of peripheral blood mononuclear cells (PBMCs), we utilized a healthy iPSC line and introduced the TTN-T32756I variant using CRISPR/Cas9 genome editing. This approach ensures an isogenic background, thereby minimizing genetic variability and providing a controlled system to study the direct effects of the mutation. We edited the genome of WT iPSCs to introduce the T32756I using CRISPR-Cas9 technique[29]. The *TTN*-T32756I CRISPR-Cas9 was designed from WT allele sgRNA and two ssODN that target the *TTN* genomic locus: 31111-31119 and genomic DNA location: chr2:178539785-178539811 (GRCh38.p13). An amplification of the exon 352 cDNA donor RNP was constructed and electroporated into *TTN* gene WT hiPSCs. Gene-editing efficiency was confirmed with next-generation sequencing (NGS). Karyotype analysis was carried out by the Cytogenetics laboratory at WiCell Research Institute Inc. Cells were collected and chromosomes were evaluated using the Giemsa trypsin Wright (GTW) banding method. Metaphase cells were analyzed, all of which were concluded to have a normal karyotype (46, XY)

Contraction analysis and optical voltage mapping

Contractility of hiPSC-aCMs was performed with a versatile open-source software, MUSCLEMOTION[65]. MUSCLEMOTION is ab ImageJ plugin that utilizes a video-based system to assess contractile functions. Optical voltage mapping recordings were performed on the IonOptix system myopacer system using the fluovolt membrane potential kit (Thermo Fisher). HiPSC-aCMs were cultured in confocal dishes were incubated with Tyrode's solution (140 mM NaCl, 4.56 mM KCl, 0.73 mM $MgCl_2$, 10 mM HEPES, 5.0 mM dextrose, 1.25 mM $CaCl_2$) plus 1x Fluovolt (Sigma/Aldrich) for 15-20 minutes. Cells were then rinsed with normal Tyrode's solution and recorded APDs on the IonOptix system. For pacing experiment, iPSC-aCMs were electrically stimulated at a frequency of 0.5 Hz with platinum wires separated 2-4 mm, stimulation voltage was 25 % above threshold (10 V, 4 msec). These experiments were performed at the room temperature (25°C).

Electrophysiology

Whole-cell patch clamping on hiPSC-aCMs I_K recordings was performed according to previously published protocols[27,29]. Briefly, voltage-clamps were achieved by using an Axopatch 200B amplifier controlled by pClamp10 software through an Axon Digidata 1440A. External solution for I_K recordings contained: 140 mM NaCl, 4 mM KCl, 1.8 mM CaCl2, 1.2 mM MgCl2, 10 mM glucose, 10 mM HEPES, and 0.01 mM nifedipine, adjusted to pH 7.4 with NaOH. I_{Ks} recordings were isolated as 1 μM HMR-1556–sensitive current. The intracellular solution contained 100 mM potassium aspartate, 2 mM MgCl2, 20 mM KCl, 5 mM Mg-ATP, 5 mM EGTA, and 10 mM HEPES adjusted to 7.2 with KOH. I_{Ks} currents were elicited by using 3-second voltage-clamp steps to test

potentials of −60 to +60 mV from holding potential of –40 mV and with 20 mV increments.

Calcium Handling

Calcium transients were measured using Fluo-4-AM (Invitrogen) dye dissolved in 2.5% Pluronic F-127 (MilliporeSigma). To get a working concentration of 5 μM, the dye solution was added to Tyrode's solution (1 mM Ca^{2+}). The cells were treated with Fluo-4-AM in 1 mM Ca^{2+} Tyrode's solution, and then allowed to sit at room temperature for 20 minutes in the dark. Tyrode's solution without indicators and containing 2 mM calcium was used to wash the cells. Using a 40× objective and the Zeiss LSM 710 confocal equipped with a BiG module, line scans were acquired and examined using ImageJ. The corrected minimum and maximum fluorescence values were determined by normalizing the fluorescence using a baseline background region that was unique to each cell. Fluorescence signals were normalized to basal cell fluorescence after fluo-4 loading (F0). For pacing experiment, iPSC-aCMs were incubated at room temperature with 1 μM Fura 2-AM for 10 min and then washed out with normal tyrode 1.8 mM Ca for 20 min. The cells were then electrically stimulated at a frequency of 0.5 Hz with platinum wires separated 2-4 mm, stimulation voltage was 25 % above threshold (10 V, 4 msec). Estimations of intracellular Ca^{2+} are reported as changes in ΔF/F0, where ΔF = F-F0. Calcium transients' amplitude (340/380 nm ratio, and kinetics were analyzed using IonOptix software.

Transmission electron microscopy (TEM)

iPSC-aCMs were fixed with 2.5% glutaraldehyde in 0.1M Sorenson's Buffer for 60 minutes at room temperature. The cells are then carefully collected into a microcentrifuge tube pre-filled with same the fixation buffer. The samples were then centrifuged at 2500xg for 10 min at room temperature. The pellet was then removed and inverted with a hypodermic needle to ensure fixative solution thoroughly permeates the sample. The pellet is then allowed to incubate at room temperature to fix for an additional 60 minutes at room temperature. The fixation solution was then removed and substituted with 1% glutaraldehyde + 4% paraformaldehyde in 0.1M Sorenson's buffer and stored in 4°C. Fixed samples were embedded in resin and microtome sections were imaged on a JEOL JEM-1400 Flash TEM.

Immunofluorescence

Cells were cultured on Matek(R) glass bottom dishes that were coated with vitronectin. The cells were then allowed to grow for a period of 2 days. The cells were then fixed with 4% paraformaldehyde (PFA) for 10 minutes and permeabilized with phosphate-buffered saline (PBS) containing 0.1% Triton X-100 for 10 minutes. After that, the cells were blocked with 3% bovine serum albumin (BSA) in PBS for 1 hour at room temperature. The staining procedure was carried out overnight at 4°C using primary antibodies that were diluted in 3% BSA in PBS. The cells were rinsed three times with PBS and then exposed to secondary antibodies (anti-mouse-FITC or anti-rabbit-PE, Santacruz, 1:1000) for one hour at room temperature. Subsequently, the cells were rinsed 3x with PBS and co-stained with 1µg/ml of DAPI. The antibodies Anti-SOX2 (Abcam, 1:200) and anti-OCT4 (Santacruz, 1:200) were used to assess the generation

of iPSCs, while anti-cTnT (Invitrogen, 1:300) and anti-Kv1.5 (Alomone labs, 1:200) were utilized to confirm the differentiation of atrial cardiomyocytes. The samples were visualized using an LSM710 Meta Confocal Microscope manufactured by Zeiss. For the co-localization experiment, anti-FHL2 antibody (Abcam, #ab202584) and anti-KCNE1 antibody (Alomone Labs, #APC-163) were used and the subsequent captured images were analyzed using ImageJ software with the Coloc2 plugin. Pearson's correlation coefficient was calculated to quantify the degree of co-localization between FHL2 and KCNE1 signals.

Protein isolation, western blotting, and co-immunoprecipitation

We performed Western blots as previously described[27,29]. For western blots, cells on 6-well plates were washed with ice cold DPBS without Ca^{2+} and Mg^{2+}, after which 250 µL of 1X RIPA with protease and phosphatase inhibitors was added per well. Lysate concentrations were measured using BCA Assay, and diluted with 4X Laemmli buffer with 10% 2-Mercaptoethanol. Per sample, 25 µg of protein was then run on an SDS-polyacrylamide gel to separate, and resolved gels were electro-transferred on 0.2 µm PVDF membranes. Membranes were blocked with 5% BSA for 1 hour, and then probed with corresponding antibodies of target proteins (anit-FHL2 antibody, Abcam#ab202584). The blots were developed using either anti-rabbit HRP or anti-mouse HRP and scanned on C280 imaging systems (Azure Biosystems). Protein signal densities were determined using ImageJ and normalized to corresponding β-actin signal densities.

For co-immunoprecipitation experiments, cells are rinsed with ice cold DPBS without Ca^{2+} and Mg^{2+}, after which 500 µL of 1X RIPA with protease and phosphatase inhibitors was added each well of a 6-well plate. Lysates are sonicated on ice 3x5 seconds, then centrifuged for 10 min at 14,000xg at 4°C. 100µL of Protein A/G agarose bead slurry was added to the lysate and incubated at 4°C on a rotator for 60 minutes. The cell lysate with bead slurry was centrifuged for 10 minutes at 1000xg at 4°C and the supernatant was transferred to a fresh Eppendorf tube. 2µg of primary antibody (Anti-KCNE1 [Alomone# APC-163]: 2.5µL) was added to 500µg of precleared cell lysate, and the mixture was incubated with gentle rotation overnight at 4°C for a day. 40µL of Protein A/G bead slurry was the washed 3x with RIPA, and the precleared cell lysate with the primary antibody was added to the bead slurry, and then followed by incubation for 3 hours at 4°C. The mixture is centrifuged for 10 min at 1000xg at 4°C, and the flow through was saved to verify the immunoprecipitation. The bead pellet was rinsed with 5x500 µL RIPA and resuspended in 30µL 4X Laemmli sample buffer, vortexed, then centrifuged for 30 seconds. The sample was then boiled for 5 min, then centrifuged at 14,000xg for 5 min, representing the IP sample. 15 µL of supernatant and immunoprecipitate samples were loaded onto a 10% SDS-PAGE gel and analyzed by western blotting.

RNA-Sequencing

The RNA was isolated using the Maxwell® RSC simplyRNA Cells Kit (Promega AS1390) according to the instructions provided by the manufacturer. Library preparation was carried out using the Universal Plus mRNA-Seq kit (NuGen 0520-A01). Briefly,

RNA underwent poly-A selection, enzymatic fragmentation, and generation of double-stranded cDNA using a mixture of Oligo (dT) and random priming. The cDNA was subjected to end repair, ligation of dual-index adaptors, strand selection, and 15 cycles of PCR amplification. The concentrations of the purified library were determined using the Qubit 1X dsDNA HS Assay Kit (Invitrogen Q33231). The libraries were then combined in equal amounts, considering the Qubit concentration and the average size determined by TapeStation. The pooled libraries were subsequently run on the MiniSeq instrument for index balancing. The ultimate, refined pool was measured using quantitative polymerase chain reaction (qPCR). The raw reads were aligned to the reference genome hg38 using the STAR alignment tool. The quantification of ENSEMBL gene expression was performed using FeatureCounts. The edgeR package was used to calculate normalized and differential expression statistics. To account for multiple testing, p-values were adjusted using the false discovery rate (FDR) correction method. We detected differentially expressed genes (DEGs) with a q value of less than 0.05 and a log 2 fold change of at least 2 between the Control and AF iPSC-aCMs. We conducted unsupervised hierarchical clustering of all genes that showed differential expression using the Euclidean distance and complete linkage method. Additionally, we created volcano plots using the R programming language. The up- and down-regulated genes were analyzed individually using the DAVID functional annotation tool against the Gene Ontology Biological Process (GO BP) database.

qPCR

Total RNA was isolated from hiPSC-aCMs using TRIzol reagent (Invitrogen), following the manufacturer's instructions to ensure the extraction of high-quality RNA. The concentration and purity of the isolated RNA were carefully assessed using a NanoDrop 2000 spectrophotometer (Thermo Fisher Scientific), with 1 µg of total RNA utilized for each reverse transcription reaction. Reverse transcription to synthesize cDNA was conducted using SuperScript III Reverse Transcriptase (Thermo Fisher Scientific). For the analysis, specific assays and primers were selected for target gene FHL2 (Forward sequence: GTGGTGTGCTTTGAGACCCTGT, Reverse sequence: GAGCAGTGGAAACAGGCTTCATG) with glyceraldehyde 3-phosphate dehydrogenase (GAPDH) serving as the normalization reference gene. qPCR reactions were performed on an ABI QuantStudio 5 system (Applied Biosystems), using SYBR Green PCR Master Mix to accurately detect and quantify PCR amplification products. Relative expression levels of the target genes were calculated employing the ΔΔCt method, by the quantification of gene expression changes in the experimental samples relative to control. For the ΔCT Calculation**,** the cycling time (CT) value of the target gene was subtracted from the CT value of GAPDH in the same sample using $\Delta CT = CT_{\text{target gene}} - CT_{\text{reference gene}}$. The ΔΔCT value was then calculated using $\Delta\Delta CT = \Delta CT_{Experimental} - \Delta CT_{Control}$. The relative expression for the gene was in turn calculated using Relative gene expression= $2^{-\Delta\Delta CT}$.

siRNA experiments

FHL2-specific siRNAs (#SR301594) or scrambled siRNAs were applied to mature hiPSC-aCMs using Lipofectamine RNAiMAX (Invitrogen, Carlsbad, CA). Opti-MEM

medium was used to dilute stock solutions of lipofectamine and siRNA, each prepared at a concentration of 10 µM. The siRNA-lipid complex was then made by mixing these solutions in a 1:1 ratio and incubated for five minutes. After adding this complex to the cells dropwise, the media was changed, and the cells were allowed to incubate for a further two days.

Data Analysis and Statistics

For clinical data, categorical variables are represented as count and percentage (%) and tested by Fisher's exact test. Continuous variables are reported as mean (standard deviation [SD]) or median and interquartile range (IQR) where specified and tested with Mann-Whitney U and Kruskal-Wallis tests. Ordinal variables were tested with Kruskal-Wallis test. Univariable and multivariable Cox proportional hazards models were used to evaluate risk of the primary outcome as recurring events, related to presence of *TTN* missense variants. A partially adjusted model was first tested using covariates of age and sex, followed by a fully adjusted model which additionally incorporated covariates of ethnicity and baseline LVEF <50%. Interaction between *TTN* missense variants and LVEF was additionally evaluated. To identify whether associations were limited to variants with predicted deleterious effect, analysis was repeated stratifying subjects according to presence and predicted impact of *TTN*mv: presence of one or more predicted deleterious (REVEL≥0.7) variants, presence of predicted benign (REVEL <0.7) variants only, or no *TTN*mv present. Additional sensitivity analyses were performed excluding subjects with multiple *TTN*mvs and with nonischemic dilated cardiomyopathy. Analysis was performed in R (version 4.2.1, packages: *arsenal,*

ggplot2, ggsurvfit, *gtsummary*, *reda*, *survival*). Experiments were performed at least two times (biological replicates) to ensure reproducibility. Unless otherwise noted, experimental data on hiPSCs are shown as mean ± SD. *P < 0.05, **P < 0.01, ***P < 0.001, ****P < 0.0001 indicate significance, while P > 0.05 is regarded as non-significant. Statistical analyses include unpaired nonparametric and 2-tailed Mann-Whitney U test for data with normal distribution, and either 1-way or 2-way ANOVA with post hoc Bonferroni's corrections for several groups. The first and third quartiles of a median are used to express skewed data. Fisher's Exact test is used to compare categorical data, and unpaired Student's t-test or ANOVA are applied to assess continuous variables.

DATA AVAILABILITY

Whole genome sequencing data of the patients are subject to conditions of the IRB protocols and UIC policies under which the data was generated, and therefore the raw sequencing data is unavailable. The ClinVar accession number for the variant studied is VCV000178164.47. Data that support the findings of this study are available from the corresponding author upon reasonable request.

CODE AVAILABILITY

R version 4.2.1 and packages (arsenal, ggplot2, ggsurvfit, gtsummary, reda, survival, tidycmprsk) are available at https://cran.r-project.org/. Variants are annotated with Ensembl Variant Effect Predictor

(https://www.ensembl.org/info/docs/tools/vep/index.html) and CardioDB (https://cardiodb.org/titin) for TTN region and percent spliced in (PSI).

REFERENCES

1. Brundel, B. J. J. M. *et al.* Atrial fibrillation. *Nature Reviews Disease Primers 2022 8:1* **8**, 1–23 (2022).
2. Elliott, A. D., Middeldorp, M. E., Van Gelder, I. C., Albert, C. M. & Sanders, P. Epidemiology and modifiable risk factors for atrial fibrillation. *Nature Reviews Cardiology 2023 20:6* **20**, 404–417 (2023).
3. Schotten, U., Verheule, S., Kirchhof, P. & Goette, A. Pathophysiological mechanisms of atrial fibrillation: A translational appraisal. *Physiol Rev* **91**, 265–325 (2011).
4. Markides, V. & Schilling, R. J. Atrial fibrillation: classification, pathophysiology, mechanisms and drug treatment. *Heart* **89**, 939 (2003).
5. Lee, D. S. M., Damrauer, S. M. & Levin, M. G. Genetics of atrial fibrillation. *Curr Opin Cardiol* **38**, 162–168 (2023).
6. Feghaly, J., Zakka, P., London, B., MacRae, C. A. & Refaat, M. M. Genetics of Atrial Fibrillation. *J Am Heart Assoc* **7**, (2018).
7. Sagris, M. *et al.* Atrial Fibrillation: Pathogenesis, Predisposing Factors, and Genetics. *Int J Mol Sci* **23**, (2022).
8. Roselli, C., Roselli, C., Rienstra, M., Ellinor, P. T. & Ellinor, P. T. Genetics of Atrial Fibrillation in 2020: GWAS, Genome Sequencing, Polygenic Risk, and Beyond. *Circ Res* **127**, 21–33 (2020).
9. Roselli, C. *et al.* Multi-ethnic genome-wide association study for atrial fibrillation. *Nature Genetics 2018 50:9* **50**, 1225–1233 (2018).
10. Choi, S. H. *et al.* Association between titin loss-of-function variants and early-onset atrial fibrillation. *JAMA* **320**, 2354 (2018).
11. Chalazan, B. *et al.* Association of Rare Genetic Variants and Early-Onset Atrial Fibrillation in Ethnic Minority Individuals. *JAMA Cardiol* (2021) doi:10.1001/jamacardio.2021.0994.
12. S Labeit, B. K. Titins: giant proteins in charge of muscle ultrastructure and elasticity. *Science (1979)* **270**, 293–296 (1995).
13. Granzier, H. L. & Labeit, S. The Giant Protein Titin: A Major Player in Myocardial Mechanics, Signaling, and Disease. *Circulation Research* vol. 94 284–295 Preprint at https://doi.org/10.1161/01.RES.0000117769.88862.F8 (2004).
14. MM LeWinter, Y. W. S. L. H. G. Cardiac titin: structure, functions and role in disease. *Clin. Chim. Acta* **375**, 1–9 (2007).
15. Linke, W. A. & Hamdani, N. Gigantic business: Titin properties and function through thick and thin. *Circulation Research* vol. 114 1052–1068 Preprint at https://doi.org/10.1161/CIRCRESAHA.114.301286 (2014).
16. Schafer, S. Titin-truncating variants affect heart function in disease cohorts and the general population. *Nat. Genet.* **49**, 46–53 (2017).

778 17. Begay, R. Role of titin missense variants in dilated cardiomyopathy. *J. Am. Heart Assoc.* **4**,
779 (2015).
780 18. Vissing, C. R. *et al.* Dilated cardiomyopathy caused by truncating titin variants: long-term
781 outcomes, arrhythmias, response to treatment and sex differences. *J Med Genet* **58**,
782 832–841 (2021).
783 19. Akinrinade, O. *et al.* Relevance of Titin Missense and Non-Frameshifting
784 Insertions/Deletions Variants in Dilated Cardiomyopathy. *Sci Rep* **9**, (2019).
785 20. Weston, T. G. R., Rees, M., Gautel, M. & Fraternali, F. Walking with giants: The challenges
786 of variant impact assessment in the giant sarcomeric protein titin. *WIREs Mechanisms of*
787 *Disease* e1638 (2023) doi:10.1002/WSBM.1638.
788 21. Martínez-barrios, E. *et al.* Discerning the Ambiguous Role of Missense TTN Variants in
789 Inherited Arrhythmogenic Syndromes. *J Pers Med* **12**, (2022).
790 22. Richards, S. *et al.* Standards and Guidelines for the Interpretation of Sequence Variants:
791 A Joint Consensus Recommendation of the American College of Medical Genetics and
792 Genomics and the Association for Molecular Pathology. *Genet Med* **17**, 405 (2015).
793 23. Domínguez, F. *et al.* Titin Missense Variants as a Cause of Familial Dilated
794 Cardiomyopathy. *Circulation* **147**, 1711–1713 (2023).
795 24. Liu, G. *et al.* Novel missense variant in TTN cosegregating with familial atrioventricular
796 block. *Eur J Med Genet* **63**, (2020).
797 25. Chen, E. *et al.* Rates and Classification of Variants of Uncertain Significance in Hereditary
798 Disease Genetic Testing. *JAMA Netw Open* **6**, E2339571 (2023).
799 26. Ly, O. T., Brown, G. E., Han, Y. D., Darbar, D. & Khetani, S. R. Bioengineering approaches
800 to mature induced pluripotent stem cell-derived atrial cardiomyocytes to model atrial
801 fibrillation. *Exp Biol Med* **246**, 1816–1828 (2021).
802 27. Ly, O. T. *et al.* Mutant ANP induces mitochondrial and ion channel remodeling in a
803 human iPSC–derived atrial fibrillation model. *JCI Insight* **7**, (2022).
804 28. Nicholson, M. W. *et al.* Utility of iPSC-Derived Cells for Disease Modeling, Drug
805 Development, and Cell Therapy. *Cells* **11**, (2022).
806 29. Hong, L. *et al.* Human induced pluripotent stem cell-derived atrial cardiomyocytes
807 carrying an SCN5A mutation identify nitric oxide signaling as a mediator of atrial
808 fibrillation. *Stem Cell Reports* **16**, 1542–1554 (2021).
809 30. Poetsch, M. S. & Guan, K. iPSCs for modeling of sarcomeric cardiomyopathies. *Recent*
810 *Advances in iPSC Disease Modeling, Volume 1* 237–273 (2020) doi:10.1016/B978-0-12-
811 822227-0.00012-0.
812 31. Li, S. *et al.* Mitochondrial Dysfunctions Contribute to Hypertrophic Cardiomyopathy in
813 Patient iPSC-Derived Cardiomyocytes with MT-RNR2 Mutation. *Stem Cell Reports* **10**,
814 808–821 (2018).
815 32. Nijak, A. *et al.* iPSC-Cardiomyocyte Models of Brugada Syndrome—Achievements,
816 Challenges and Future Perspectives. *International Journal of Molecular Sciences 2021,*
817 *Vol. 22, Page 2825* **22**, 2825 (2021).
818 33. Moretti, A. *et al.* Patient-Specific Induced Pluripotent Stem-Cell Models for Long-QT
819 Syndrome. *New England Journal of Medicine* **363**, 1397–1409 (2010).

820 34. Benzoni, P. *et al.* Human iPSC modelling of a familial form of atrial fibrillation reveals a
821 gain of function of If and ICaL in patient-derived cardiomyocytes. *Cardiovasc Res* **116**,
822 1147 (2020).
823 35. Simons, E., Loeys, B. & Alaerts, M. iPSC-Derived Cardiomyocytes in Inherited Cardiac
824 Arrhythmias: Pathomechanistic Discovery and Drug Development. *Biomedicines* **11**,
825 (2023).
826 36. Brown, G. E. *et al.* Engineered cocultures of iPSC-derived atrial cardiomyocytes and atrial
827 fibroblasts for modeling atrial fibrillation. *Sci Adv* **10**, (2024).
828 37. Jiang, X. *et al.* Transient titin-dependent ventricular defects during development lead to
829 adult atrial 1 arrhythmia and impaired contractility 2 3 Corresponding Authors 25.
830 *Iscience (In press)* (2024).
831 38. Schick, R. *et al.* Functional abnormalities in induced Pluripotent Stem Cell-derived
832 cardiomyocytes generated from titin-mutated patients with dilated cardiomyopathy.
833 *PLoS One* **13**, (2018).
834 39. Hinson, J. T. *et al.* Titin Mutations in iPS cells Define Sarcomere Insufficiency as a Cause of
835 Dilated Cardiomyopathy. *Science* **349**, 982 (2015).
836 40. Nattel, S., Heijman, J., Zhou, L. & Dobrev, D. Molecular Basis of Atrial Fibrillation
837 Pathophysiology and Therapy. *Circ Res* 51–72 (2020)
838 doi:10.1161/CIRCRESAHA.120.316363.
839 41. McCauley, M. D. *et al.* Ion Channel and Structural Remodeling in Obesity-Mediated Atrial
840 Fibrillation. *Circ Arrhythm Electrophysiol* **13**, 8296 (2020).
841 42. Menon, A. *et al.* Electrophysiologic and molecular mechanisms of a frameshift NPPA
842 mutation linked with familial atrial fibrillation. *J Mol Cell Cardiol* **132**, 24–35 (2019).
843 43. Kupershmidt, S. *et al.* Cardiac-enriched LIM domain protein fhl2 is required to generate
844 IKs in a heterologous system. *Cardiovasc Res* **56**, 93–103 (2002).
845 44. Goodyer, W. R. *et al.* Broad Genetic Testing in a Clinical Setting Uncovers a High
846 Prevalence of Titin Loss-of-Function Variants in Very Early Onset Atrial Fibrillation. *Circ*
847 *Genom Precis Med* **12**, 526–528 (2019).
848 45. Yoneda, Z. T. *et al.* Early-Onset Atrial Fibrillation and the Prevalence of Rare Variants in
849 Cardiomyopathy and Arrhythmia Genes. *JAMA Cardiol* **6**, 1371–1379 (2021).
850 46. Choi, S. H. *et al.* Monogenic and Polygenic Contributions to Atrial Fibrillation Risk: Results
851 from a National Biobank. *Circ Res* **126**, 200 (2020).
852 47. Roberts, A. M. *et al.* Integrated allelic, transcriptional, and phenomic dissection of the
853 cardiac effects of titin truncations in health and disease. *Sci Transl Med* **7**, (2015).
854 48. Akinrinade, O., Alastalo, T. P. & Koskenvuo, J. W. Relevance of truncating titin mutations
855 in dilated cardiomyopathy. *Clin Genet* **90**, 49–54 (2016).
856 49. Kapoor, A. *et al.* Rare coding TTN variants are associated with electrocardiographic QT
857 interval in the general population. *Sci Rep* **6**, (2016).
858 50. Richards, S. *et al.* Standards and guidelines for the interpretation of sequence variants: a
859 joint consensus recommendation of the American College of Medical Genetics and
860 Genomics and the Association for Molecular Pathology. *Genetics in Medicine* **17**, 405–
861 424 (2015).

862 51. Li, H., Carrion-Vazquez, M., Oberhauser, A. F., Marszalek, P. E. & Fernandez, J. M. Point
863 mutations alter the mechanical stability of immunoglobulin modules. *Nat Struct Biol* **7**,
864 1117–1120 (2000).
865 52. Zuo, J., Zhan, D., Xia, J. & Li, H. Single-Molecule Force Spectroscopy Studies of Missense
866 Titin Mutations That Are Likely Causing Cardiomyopathy. *Langmuir* **37**, 12128–12137
867 (2021).
868 53. Anderson, B. R., Bogomolovas, J., Labeit, S. & Granzier, H. Single Molecule Force
869 Spectroscopy on Titin Implicates Immunoglobulin Domain Stability as a Cardiac Disease
870 Mechanism. *J Biol Chem* **288**, 5303 (2013).
871 54. Krüger, M. & Linke, W. A. The giant protein titin: A regulatory node that integrates
872 myocyte signaling pathways. *Journal of Biological Chemistry* vol. 286 9905–9912 Preprint
873 at https://doi.org/10.1074/jbc.R110.173260 (2011).
874 55. Tran, M. K., Kurakula, K., Koenis, D. S. & de Vries, C. J. M. Protein–protein interactions of
875 the LIM-only protein FHL2 and functional implication of the interactions relevant in
876 cardiovascular disease. *Biochimica et Biophysica Acta (BBA) - Molecular Cell Research*
877 **1863**, 219–228 (2016).
878 56. Sun, Y., Liu, X., Huang, W., Le, S. & Yan, J. Structural domain in the Titin N2B-us region
879 binds to FHL2 in a force-activation dependent manner. *Nature Communications 2024*
880 *15:1* **15**, 1–14 (2024).
881 57. Liang, Y., Bradford, W. H., Zhang, J. & Sheikh, F. Four and a half LIM domain protein
882 signaling and cardiomyopathy. *Biophys Rev* **10**, 1073 (2018).
883 58. Henderson, C. A., Gomez, C. G., Novak, S. M., Mi-Mi, L. & Gregorio, C. C. Overview of the
884 Muscle Cytoskeleton. *Compr Physiol* **7**, 891 (2017).
885 59. Lang, R. M. *et al.* Recommendations for cardiac chamber quantification by
886 echocardiography in adults: an update from the American Society of Echocardiography
887 and the European Association of Cardiovascular Imaging. *J Am Soc Echocardiogr* **28**, 1-
888 39.e14 (2015).
889 60. Ioannidis, N. M. *et al.* REVEL: An Ensemble Method for Predicting the Pathogenicity of
890 Rare Missense Variants. *Am J Hum Genet* **99**, 877 (2016).
891 61. Morales, A. *et al.* Variant Interpretation for Dilated Cardiomyopathy: Refinement of the
892 American College of Medical Genetics and Genomics/ClinGen Guidelines for the DCM
893 Precision Medicine Study. *Circ Genom Precis Med* **13**, E002480 (2020).
894 62. McLaren, W. *et al.* The Ensembl Variant Effect Predictor. *Genome Biol* **17**, 1–14 (2016).
895 63. Roberts, A. M. *et al.* Integrated allelic, transcriptional, and phenomic dissection of the
896 cardiac effects of titin truncations in health and disease. *Sci Transl Med* **7**, (2015).
897 64. Argenziano, M. *et al.* Electrophysiologic Characterization of Calcium Handling in Human
898 Induced Pluripotent Stem Cell-Derived Atrial Cardiomyocytes. *Stem Cell Reports* **10**, 1867
899 (2018).
900 65. Sala, L. *et al.* Musclemotion: A versatile open software tool to quantify cardiomyocyte
901 and cardiac muscle contraction in vitro and in vivo. *Circ Res* **122**, e5–e16 (2018).
902

903

FIGURE LEGENDS

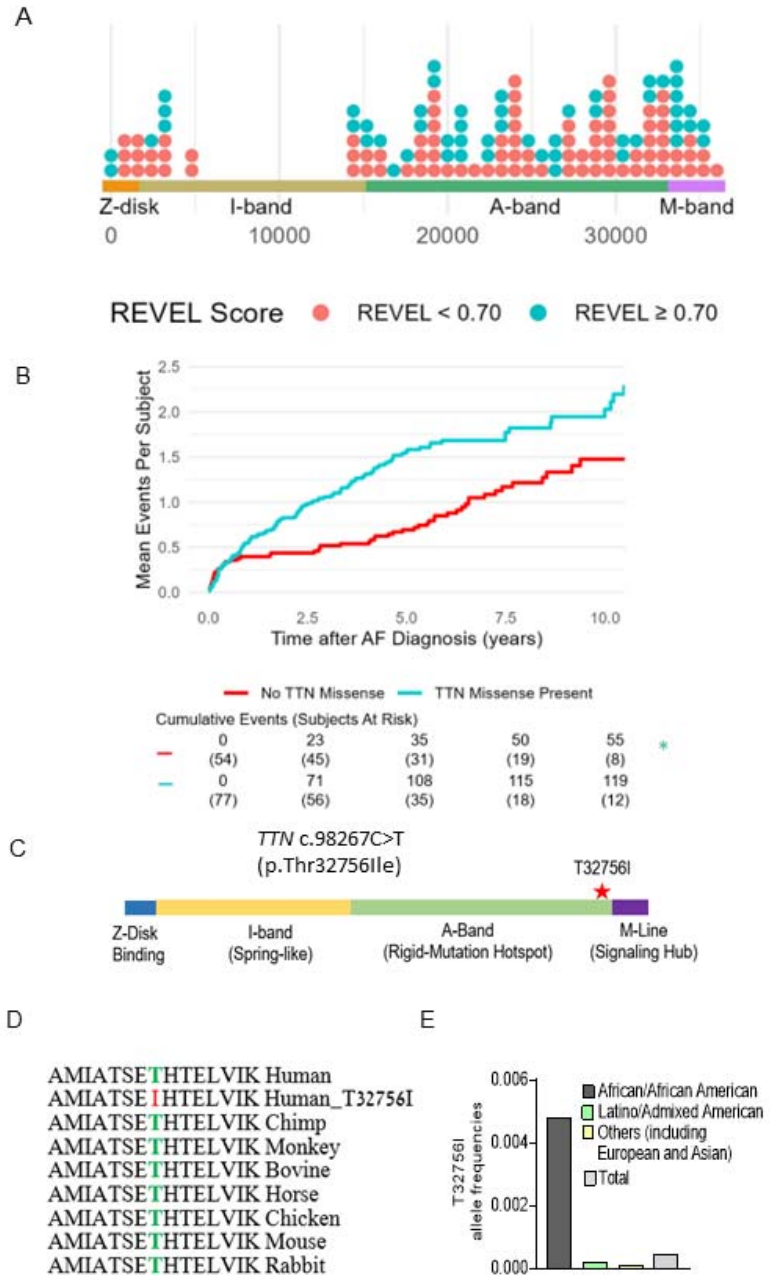

Figure 1: *TTN*mv prevalence and association with hospitalization in a multiethnic atrial fibrillation (AF) cohort. (A) Distribution of *TTN*mvs in a multiethnic AF cohort based on amino acid position in the *TTN* gene, stratified by REVEL *in silico* score for prediction of deleterious effect, defined by REVEL ≥ 0.70. (B) Mean cumulative

incidence of AF and heart failure (HF)-related hospitalizations in subjects with AF stratified by presence of *TTN*mv. Hazard ratio (HR), 95% confidence interval (CI), and P-value were obtained from univariable Cox proportional hazard modeling. (C) Diagram denoting the location of *TTN*mv-T23756I. (D) Sequence alignment shows that the T23756I region is highly conserved across vertebrate species. (E) Allele frequencies of *TTN*-T3265I in various ethnic groups (gnomAD).

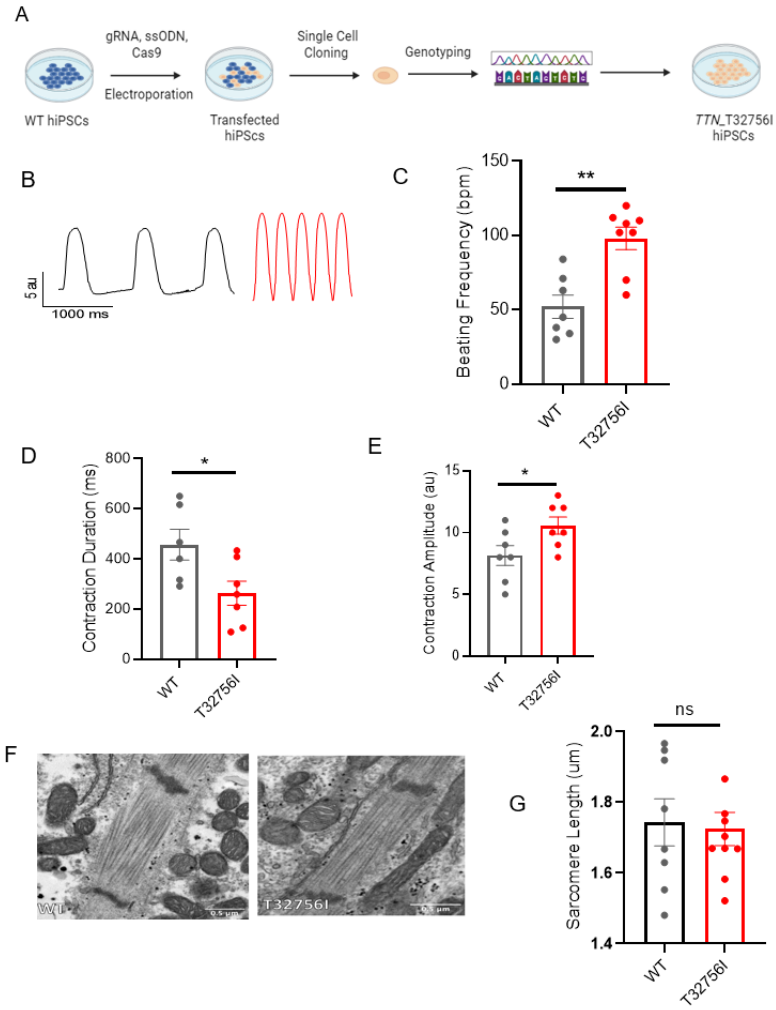

Figure 2: Human-induced pluripotent stem cell-derived atrial cardiomyocytes (iPSC-aCMs) carrying TTN-T32756I variants exhibit atypical contractility but no sarcomere disorganization. (A) Workflow for generating the CRISPR/Cas9-mediated iPSC line carrying the *TTN*-T32756I missense variation. (B-E) Contraction profile of wild type (black) and *TTN*-T32756I (Red) iPSC-aCMs (B) showing increased beating frequency (C), decreased contraction duration (D), and increased contraction amplitude (E) in the mutant. (F) Representative sarcomeric organization of wild-type (WT) and *TTN*-T32756I iPSC-aCM by Transmission electron microscopy (TEM). (G) There is no significant change in the sarcomere length. n.s. P>0.05; *P<0.05; **P< 0.01.

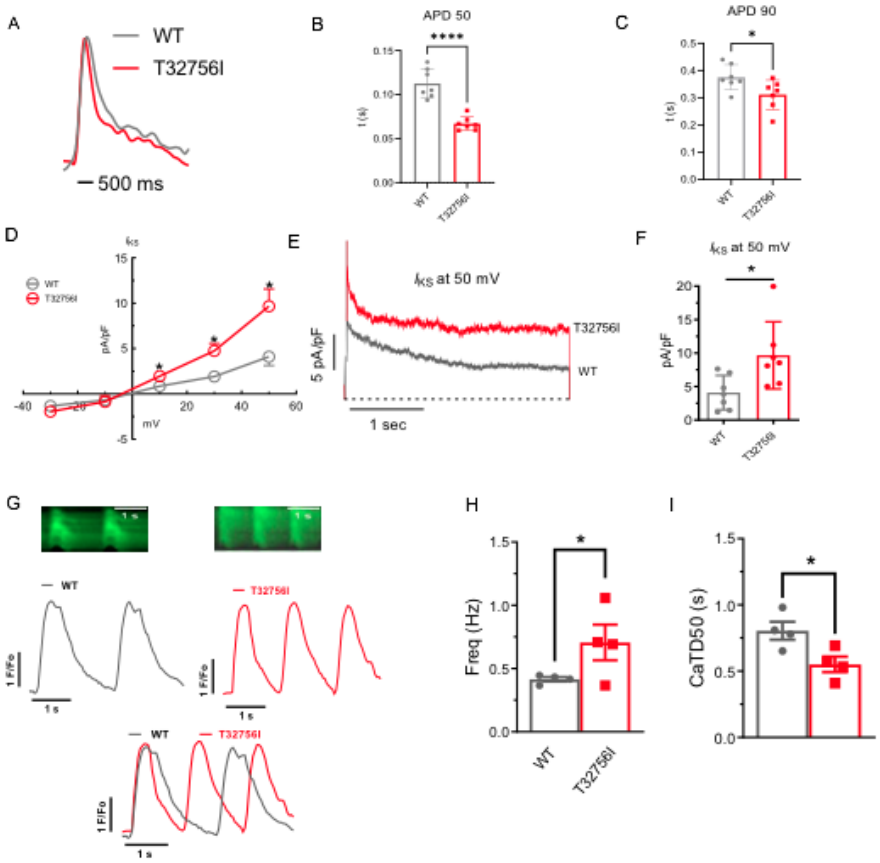

Figure 3: Effect of T32756I on action potential (AP) and calcium-handling in iPSC-aCMs. (A-C) Representative optical AP recordings of spontaneously beating WT (A) and *TTN*-T32756I showing reduction of AP duration (APD) at the 50% (APD50) (B) and 90% (APD90) repolarization (C). (D) Current-voltage (I-V) curves of the slow delayed rectifier potassium current (I_{ks}) in WT and *TTN*_T32756I iPSC-aCMs (n=7). (E-F) Comparison of I_{ks} current density at 50 mV (mean ± SEM). (G) Representative tracings of spontaneous calcium transients of WT and *TTN*-T32756I iPSC-aCMs. (H-I) Calcium kinetics show that the *TTN*-T32756I iPSC-aCMs have increased frequency (H) and decreased transient durations (I) compared with the WT iPSC-aCMs. n.s. P>0.05; *P<0.05.

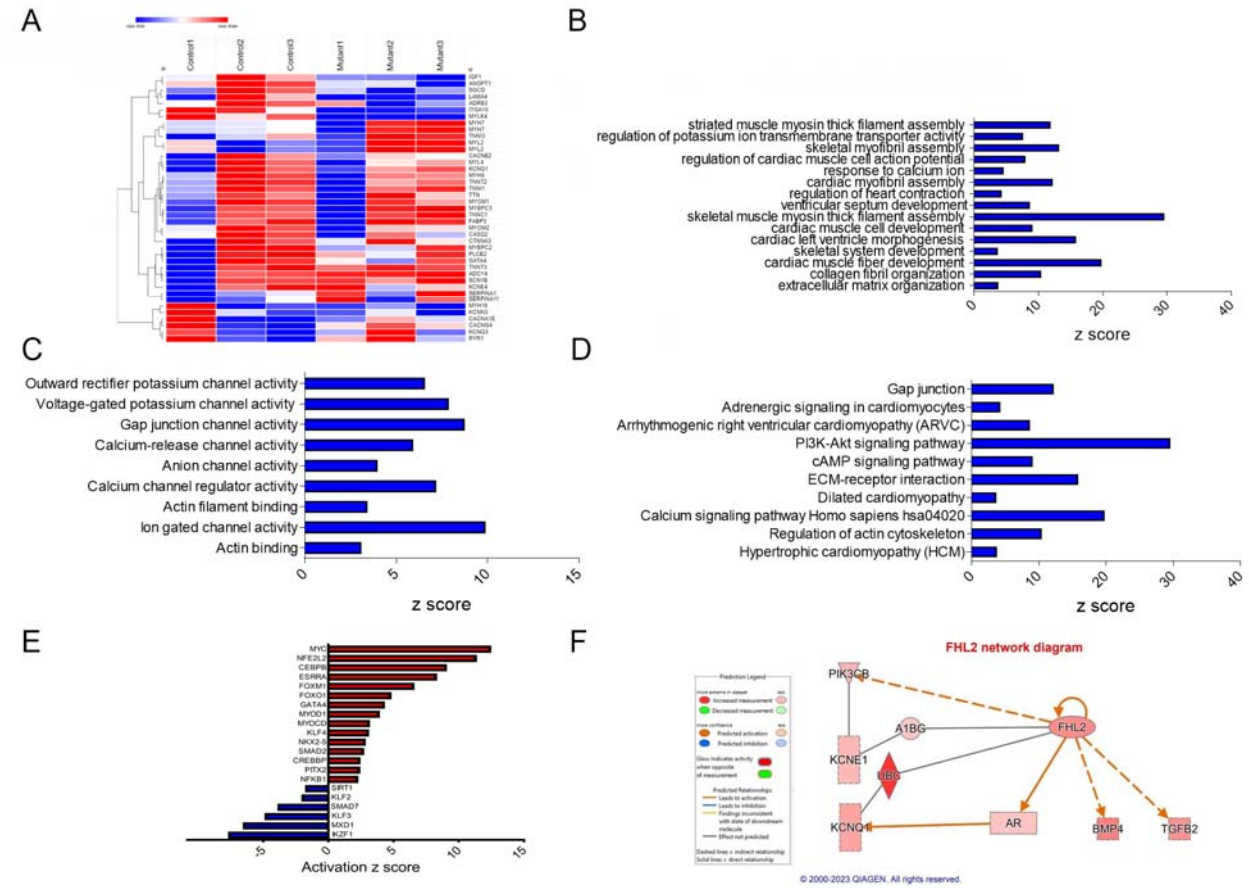

Figure 4: Transcriptomic profile and pathway enrichment analysis comparing *TTN*-T32756I iPSC-aCMs with the WT. (A) Heatmaps of cardiac-related upregulated and downregulated differentially expressed genes (DEGs). (B) Top significantly enriched downregulated cardiac-related Gene-Ontology Biological process (GO-BP) pathways in the *TTN*-T32756I iPSC-aCMs. (C) Top significantly enriched downregulated cardiac-related Gene-Ontology Molecular Function (GO-MF) pathways in the *TTN*-T32756I iPSC-aCMs. (D) Top significantly enriched downregulated cardiac-related Kyoto Encyclopedia of Genes and Genomes (KEGG) pathways in the *TTN*-T32756I iPSC-aCMs. (E) Significantly enriched upregulated and downregulated transcription factors (TFs). (F) Network diagram showing the upregulation of KCNQ1 by FHL2 predicted by the Ingenuity pathway enrichment analysis (IPA).

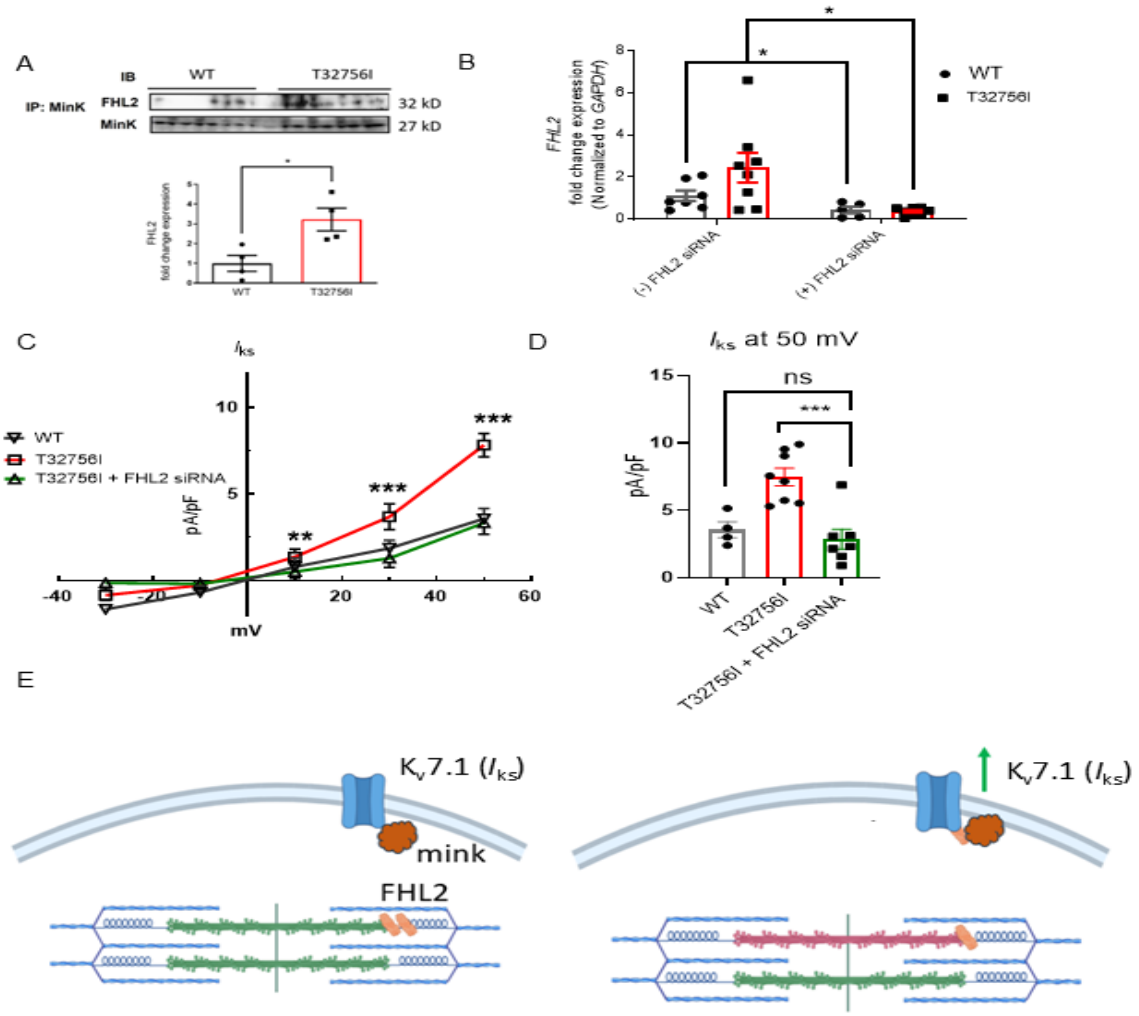

Figure 5: Inhibition of FHL2 rescues enhanced I_{ks} in *TTN*-T32756I iPSC-aCMs. (A) Co-immunoprecipitation revealed increased interaction between FHL2 and KCNQ1-KCNE1 (MinK) complex. (IP: KCNE1). Immunoblotting (IB) was performed with antibodies against FHL2 (32 kDa) and MinK (32 kDa) (n = 3) (B) qPCR data showing the inhibition of *FHL2* gene by the siRNA in the WT and *TTN*-T32756I iPSC-aCMs (n=7). (C) I-V curves showing the rescue of the I_{ks} *TTN*-T32756I iPSC-aCMs by the suppression of FHL2 (n=4-8). (D) Comparison of I_{ks} current density at 50 mV (mean ± SEM). (E) Schematic showing the *TTN*-T32756I results in increased FHL2 binding with

the KNCQ1-KCNE1 complex and enhanced I_{ks} activity. n.s. P>0.05; *P<0.05; ***P<0.001.

	***TTN* Missense Absent** (N=54)	***TTN* Missense Present** (N=77)	**Total** (N=131)	**P-value**
Age at AF diagnosis (years)	64.3 (15.2)	62.9 (12.9)	63.5 (13.8)	0.575
Male sex	30 (55.6%)	40 (51.9%)	70 (53.4%)	0.724
Race/ethnicity				0.696
Non-Hispanic Black	37 (68.5%)	56 (72.7%)	93 (71.0%)	
Hispanic/Latinx	17 (31.5%)	21 (27.3%)	38 (29.0%)	
BMI (kg/m^2)	33.7 (9.0)	34.2 (10.1)	34.0 (9.6)	0.765
Diabetes	18 (33.3%)	32 (41.6%)	50 (38.2%)	0.366
Hypertension	45 (83.3%)	68 (88.3%)	113 (86.3%)	0.448
Coronary artery disease	13 (24.1%)	20 (26.0%)	33 (25.2%)	0.841
History of stroke/transient ischemic attack	8 (14.8%)	18 (23.4%)	26 (19.8%)	0.270
Congestive heart failure	21 (38.9%)	33 (42.9%)	54 (41.2%)	0.720
Nonischemic dilated cardiomyopathy	4 (7.7%)	8 (11.1%)	12 (9.7%)	0.760
Estimated glomerular filtration rate (mg/dL)	71.8 (24.4)	67.2 (24.7)	69.1 (24.6)	0.297
Ventricular rate	92.1 (29.0)	97.5 (29.6)	95.3 (29.4)	0.326
QRS interval (ms)	97.6 (23.7)	100.2 (28.1)	99.2 (26.3)	0.593
QTc interval (ms)	449.6 (37.7)	466.5 (42.3)	459.6 (41.2)	0.027
Left ventricular ejection fraction (%)				0.722
Normal (≥50%)	32 (59.3%)	45 (58.4%)	77 (58.8%)	
Mildly decreased (40-49%)	7 (13.0%)	7 (9.1%)	14 (10.7%)	
Moderately decreased (30-39%)	4 (7.4%)	9 (11.7%)	13 (9.9%)	
Severely decreased (20-29%)	7 (13.0%)	9 (11.7%)	16 (12.2%)	
Very severely decreased (< 20%)	4 (7.4%)	7 (9.1%)	11 (8.4%)	
Left ventricular end diastolic diameter (mm)	45.3 (9.2)	47.8 (9.8)	46.7 (9.5)	0.180
Left ventricular dilatation	4 (8.3%)	13 (20.3%)	17 (15.2%)	0.111
Left atrial size				0.675
Normal	17 (32.7%)	21 (28.8%)	38 (30.4%)	
Mildly dilated	15 (28.8%)	23 (31.5%)	38 (30.4%)	
Moderately dilated	13 (25.0%)	17 (23.3%)	30 (24.0%)	
Severely dilated	7 (13.5%)	12 (16.4%)	19 (15.2%)	
Left atrial diameter (mm)	39.6 (7.4)	41.2 (7.7)	40.5 (7.6)	0.286
Number of TTN missense variants				-
0	54 (100.0%)	0 (0.0%)	54 (41.2%)	
1	0 (0.0%)	37 (48.1%)	37 (28.2%)	
2	0 (0.0%)	26 (33.8%)	26 (19.8%)	
>2	0 (0.0%)	14 (18.2%)	14 (10.7%)	
Number of predicted deleterious TTN missense variants				-
0	54 (100.0%)	34 (44.2%)	88 (67.2%)	
1	0 (0.0%)	34 (44.2%)	34 (26.0%)	
2	0 (0.0%)	9 (11.7%)	9 (6.9%)	

Table 1: Clinical characteristics of ethnic minority subjects with AF stratified by presence of rare missense TTN variants. *Data are missing for the following variables: eGFR (1), electrocardiogram within 3 months of AF diagnosis (11), LVEDD

(19), left atrial size (6), left atrial diameter (21). Left ventricular dilatation is defined as left ventricular end diastolic diameter greater than 2 standard deviations above the normal sex-specific mean value. Variants with a REVEL score ≥ 0.7 were defined as predicted deleterious. Continuous data are represented as mean (standard deviation) and categorical data are represented as count (%).

	Case 1	Case 2	Case 3
Age range at diagnosis (years)	50-54	60-64	35-39
Sex	Male	Female	Male
Race/ethnicity	Hispanic	Black	Black
Body mass index (kg/m^2)	42.2	26.9	31.4
Type	Paroxysmal	Paroxysmal	Paroxysmal
Comorbidities	Hypertension Prostate cancer	Hypertension Hyperlipidemia Coronary artery disease Uterine/vulva cancer Severe mitral regurgitation	Hypertension Asthma
Family history	No	No	No
Presenting symptoms	Asymptomatic, found during preoperative evaluation	Asymptomatic, in setting of gastrointestinal bleed	Palpitations, dyspnea
LA size (mm)	51	33	35
LVEF (%)	55	50	60
Antiarrhythmic	No	No	No
Ablation	Yes	No	No
Cardioversion	Yes	No	Yes

Table 2: Clinical characteristics of the early-onset AF patients with *TTN*-T32756I variation.

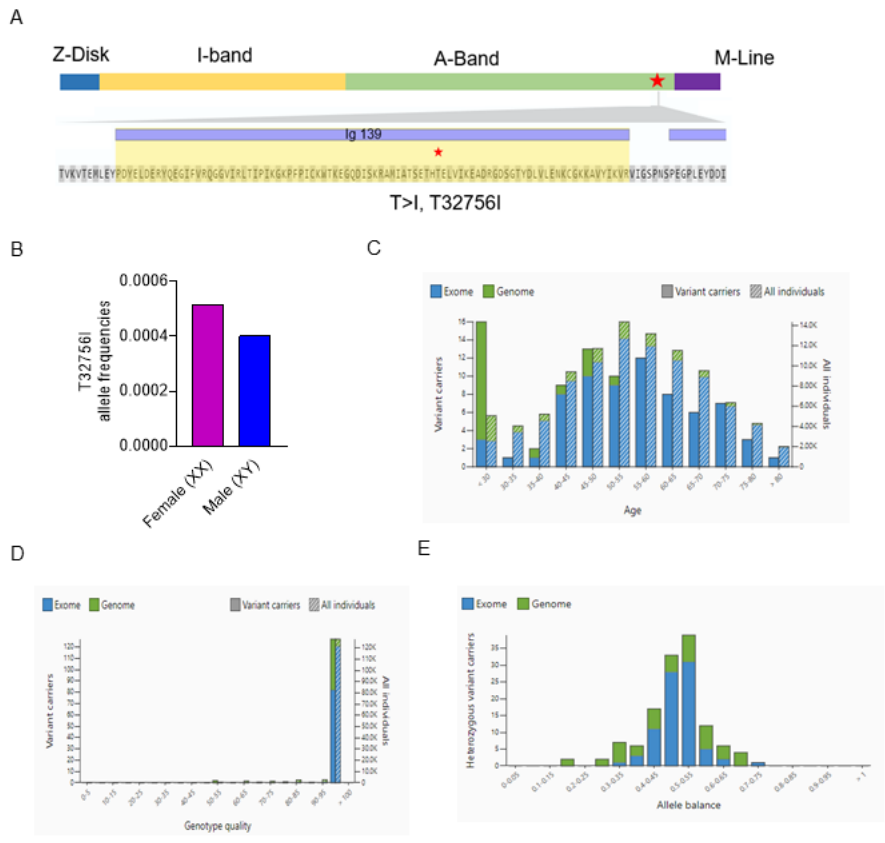

Supplementary Figure 1: *TTN*-T32756I position and distribution. (A) Location of the T23756I at Ig139 domain in the A-band of titin. (B) Allele frequencies of T3265I between sexes. (C) Age distribution of the variant carriers. (D) Genotype quality. (E) Allele balance for heterozygotes. Source: https://gnomad.broadinstitute.org/variant/2-179404525-G-A?dataset=gnomad_r2_1.

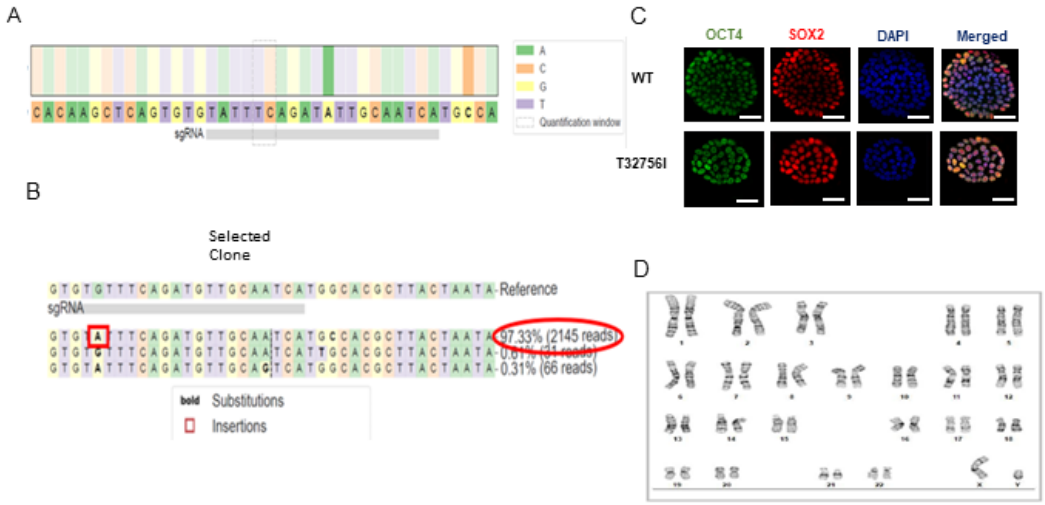

Supplementary Figure 2: Generation of iPSC-aCMs with *TTN*-T32756I. (A) *TTN* gene locus for the generation of isogenic iPSCs with the T32756I variation. Guide sequence (gRNA) shown in the bottom gray box was cloned into the vector to express gRNA guiding Cas9 exonuclease to the targeted protospacer adjacent motif sequence. (B) Next-generation sequencing of the confirming T32756I mutation. (C) Representative immunostaining of pluripotency markers OCT4 and SOX2 in iPSCs. The 4′,6-diamidino-2-phenylindole (DAPI) indicates the nucleus. (D) Karyotype analysis of the T32756I iPSCs.

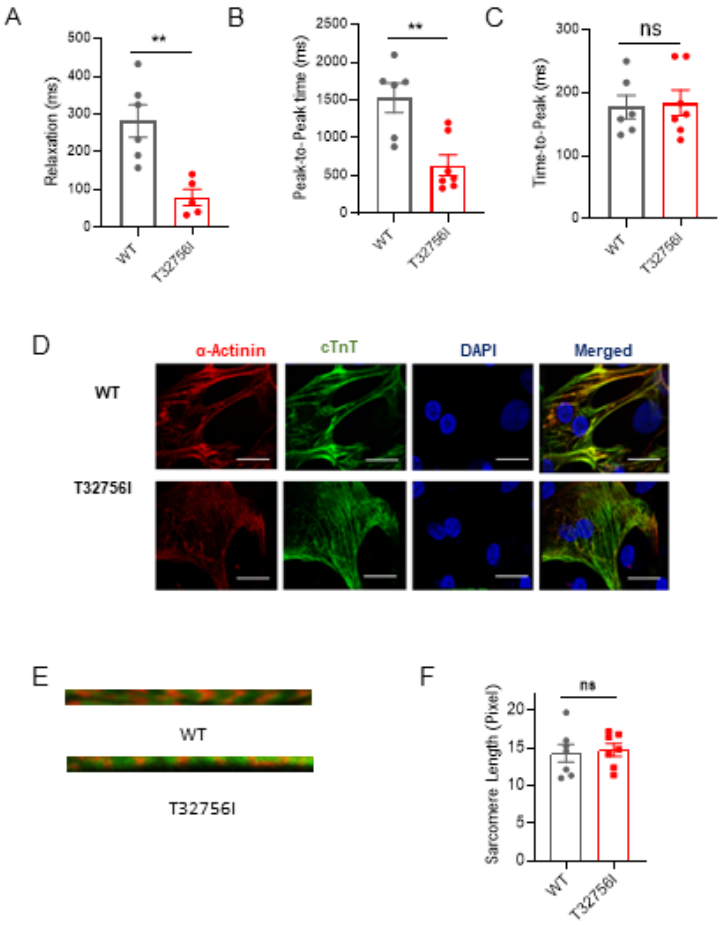

Supplementary Figure 3: Contractility and sarcomere organization of *TTN*-T32756I iPSC-aCMs. (A-C) Compared to WT, *TTN*-T32756I (Red) iPSC-aCMs show decreased relaxation time (A) and peak-to-peak time (B), but no significant change to time-to-peak (C). (D-E) Immunostaining showing the sarcomeric organization of WT and *TTN*-T32756I iPSC-aCM by the pan-cardiomyocyte (CM) marker cardiac troponin T (cTnT; green) and α-actinin (orange). The DAPI staining indicates the nucleus. (F) Bar graph showing no change in the sarcomere length. n.s. P>0.05; **P<0.01.

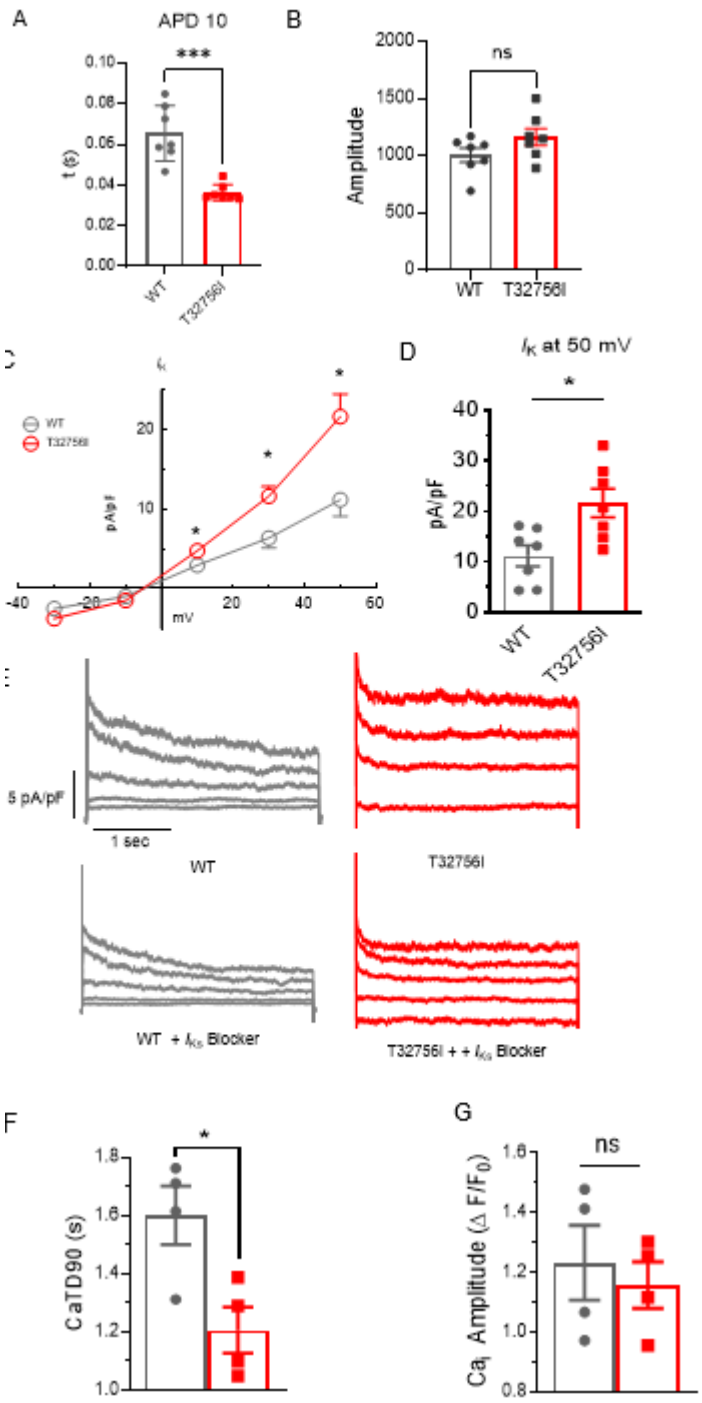

Supplementary Figure 4: *TTN*-T32756I iPSC-aCMs display anomalous action potentials, potassium currents, and calcium-handling. (A) Compared to the WT, *TTN*-T32756I shows reduction of action potential duration at the 10% (APD10) repolarization. (B) Bar graph showing no change in the amplitude of the AP. (C) Total

potassium current (I_K) and voltage relationship (I-V curves) in WT and *TTN*-T32756I iPSC-aCMs. (D) Total I_K current density at 50 mV. (E) Representative current traces at different voltages showing the isolation of the I_{ks} current with the selective blocker HMR-1556 in both WT and *TTN*-T32756I iPSC-aCMs. (F-G) Bar graph showing that the *TTN*-T32756I iPSC-aCMs have decreased transient durations (F), but no change in the transient peak amplitudes (G) compared with the WT iPSC-aCMs. n.s. P>0.05; *P<0.05; ***P<0.001.

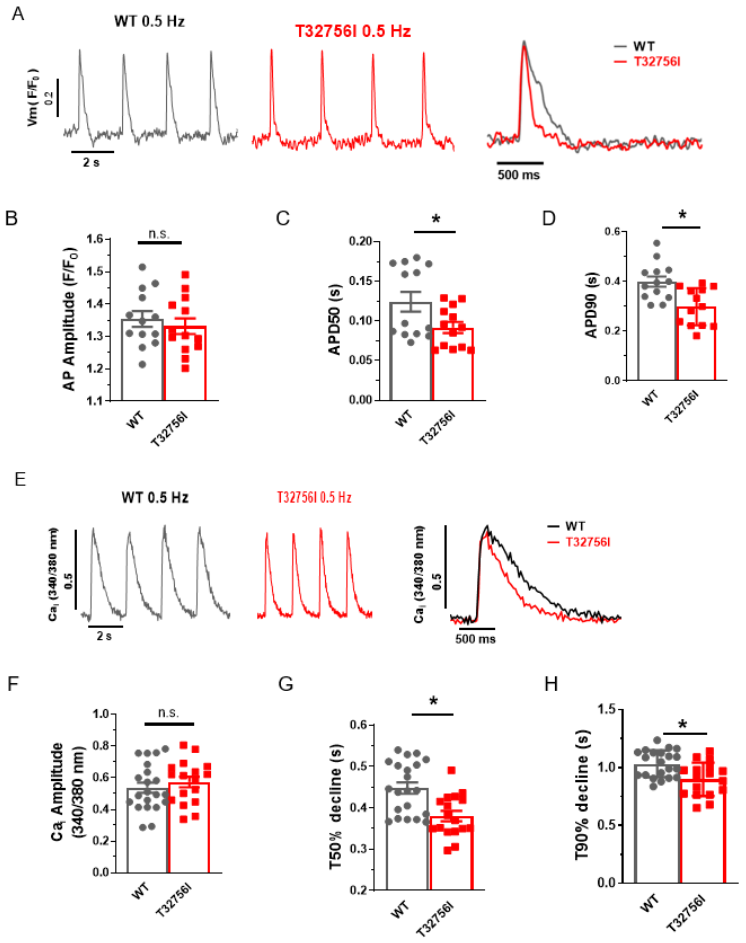

Supplementary Figure 5: Effect of T32756I on action potential and calcium-handling in paced iPSC-aCMs. (A) Representative optical AP recordings of paced (0.5 Hz) WT and *TTN*-T32756I showing reduction of AP duration (APD). (B) Bar graph showing no change in the amplitude of the AP. (C) APD50 (D) APD90. (D) Representative tracings of paced calcium transients (0.5 Hz) of WT and *TTN*-T32756I iPSC-aCMs. (E) No change in the transient peak amplitudes. (F-G). Decreased transient durations (I) in *TTN*-T32756I iPSC-aCMs compared with the WT iPSC-aCMs. n.s. P>0.05; *P<0.05.

(A) Compared to the WT, *TTN*-T32756I shows reduction of action potential duration at the 10% (APD10) repolarization. (B) Bar graph showing no change in the amplitude of the AP. (C) Total potassium current (I_K) and voltage relationship (I-V curves) in WT and *TTN*-T32756I iPSC-aCMs. (D) Total I_K current density at 50 mV. (E) Representative current traces at different voltages showing the isolation of the I_{ks} current with the selective blocker HMR-1556 in both WT and *TTN*-T32756I iPSC-aCMs. (F-G) Bar graph showing that the *TTN*-T32756I iPSC-aCMs have decreased transient durations (F), but no change in the transient peak amplitudes (G) compared with the WT iPSC-aCMs. n.s. $P>0.05$; *$P<0.05$.

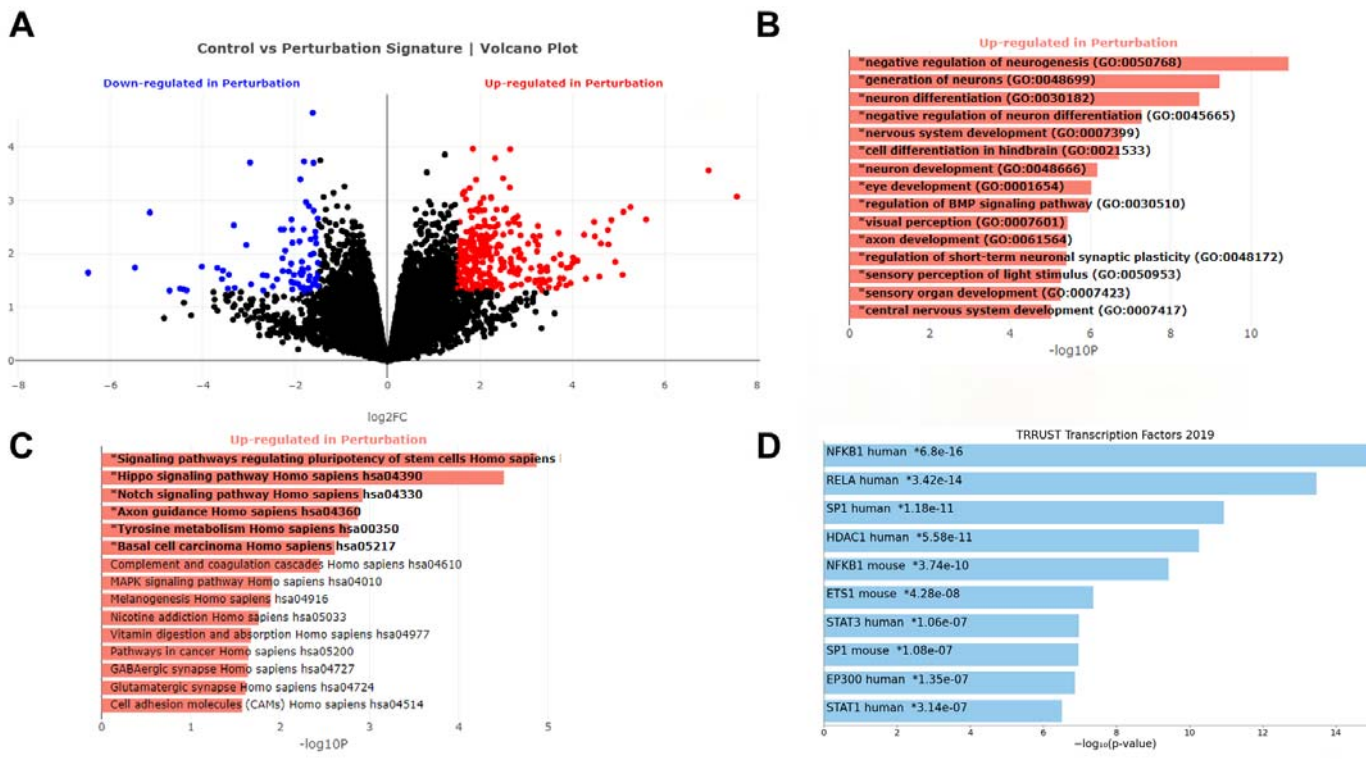

Supplementary Figure 6: Upregulated pathways in *TTN*-T32756I iPSC-aCMs with the WT. (A) Volcano plot showing spread of downregulated and upregulated differentially expressed genes (DEGs) (B) Top significantly enriched upregulated Gene-Ontology Biological process (GO-BP) pathways in the *TTN*-T32756I iPSC-aCMs. (C) Top significantly enriched upregulated Kyoto Encyclopedia of Genes and Genomes (KEGG) pathways in the *TTN*-T32756I iPSC-aCMs. (D) Top significantly enriched TTRUST transcription factors (TFs).

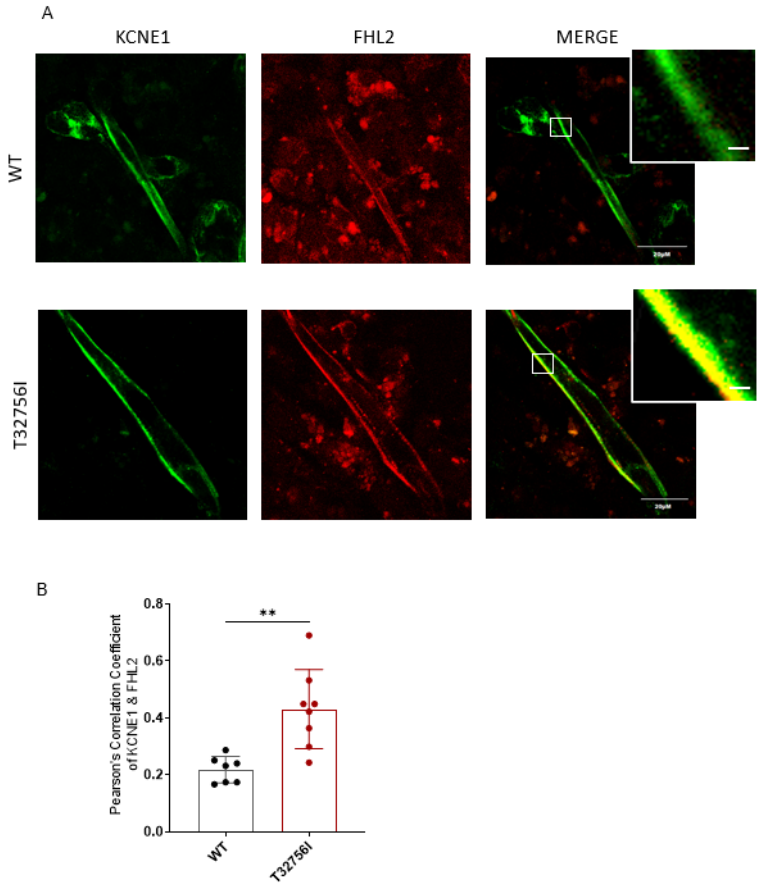

Supplementary Figure 7: Increased FHL2-KCNE1 co-localization in TTN-T32756I iPSC-aCMs. (A) Representative confocal immunofluorescence images showing subcellular localization of FHL2 (red) and KCNE1 (green) in WT and *TTN*-T32756I iPSC-aCMs. (B) Quantitative co-localization analysis, assessed by Pearson's correlation coefficient, demonstrated a significant increase in FHL2–KCNE1 co-localization in *TTN*-T32756I iPSC-aCMs compared with WT. **P < 0.01.

Subject ID	Age	Sex	Race-Ethnicity	Nucleotide	Amino Acid Change	dbSNP	gnomAD Allele Frequency	Exon	Band	Percent Spliced In (PSI)	REVEL Score
1	55-59	F	NHB	c.70250T>C	p.Ile23417Thr	rs201836227	0.000221	326	A-band	100	0.66297
2	50-54	M	HL	c.52022G>A	p.Arg17341Gln	rs370390570	0.000116	273	A-band	100	0.60691
3	50-54	M	HL	c.62519G>A	p.Gly20840Asp	rs1326564200	0.000012	304	A-band	100	0.883
4	55-59	M	NHB	c.59248G>A	p.Gly19750Ser	rs200732032	0.000109	300	A-band	100	0.75279
5	55-59	M	NHB	c.58363G>A	p.Gly19455Ser	rs191927501	0.000157	297	A-band	100	0.80842
6	65-69	M	HL	c.57727G>C	p.Ala19243Pro	rs1313667626	0.000004	295	A-band	100	0.81369
7	40-44	F	NHB	c.101665G>A	p.Val33889Ile	rs34924609	0.003099	358	A-band	100	0.17295
8	40-44	F	NHB	c.6959G>A	p.Arg2320His	rs374615369	0.000076	30	I-band	100	0.82403
9	55-59	M	NHB	c.42145G>T	p.Val14049Leu	rs1206523368			I-band	100	0.73517
10	60-64	M	NHB	c.67808C>T	p.Ala22603Val	rs199583938	0.000036	320	A-band	100	0.42028
11	60-64	M	NHB	c.101557A>G	p.Lys33853Glu	rs727505163	0.000004	358	A-band	100	0.75074
12	75-79	F	NHB	c.93266G>A	p.Arg31089His	rs367993101	0.000028	339	A-band	100	0.87283
13	75-79	F	NHB	c.970C>T	p.Pro324Ser	rs72647845	0.000598	7	Z-disk	100	0.70603
14	55-59	M	HL	c.89426G>A	p.Arg29809Gln	rs72648238	0.000632	334	A-band	100	0.45592
15	55-59	M	HL	c.99433C>T	p.Arg33145Trp	rs1338284042	0.000004	355	A-band	100	0.61955
16	75-79	M	NHB	c.74870A>G	p.Lys24957Arg	rs760043791	0.000004	326	A-band	100	0.43483
17	75-79	M	NHB	c.70817T>C	p.Met23606Thr	rs371030086	0.000040	326	A-band	100	0.624
18	80-84	F	NHB	c.101665G>A	p.Val33889Ile	rs34924609	0.003099	358	A-band	100	0.17295
19	35-39	F	NHB	c.96605T>C	p.Val32202Ala	rs763365622	0.000004	347	A-band	100	0.54781
20	35-39	F	NHB	c.70543T>G	p.Tyr23515Asp				A-band	100	0.67962
21	65-69	M	NHB	c.4671G>A	p.Met1557Ile	rs139192633	0.000272	27	near Z-disk	100	0.26882
22	65-69	F	NHB	c.91937A>G	p.Asn30646Ser	rs72648245	0.000568	338	A-band	100	0.71558
23	65-69	F	NHB	c.46693G>T	p.Ala15565Ser	rs145520397	0.000445	250	I-band	100	0.51417
24	65-69	F	NHB	c.100396C>T	p.Arg33466Cys	rs371908649	0.000145	357	A-band	100	0.8849
25	65-69	F	NHB	c.56693G>A	p.Arg18898His	rs572453785	0.000051	291	A-band	100	0.29647
26	45-49	M	NHB	c.82061T>G	p.Val27354Gly	rs368023868	0.000036	326	A-band	100	0.77847
27	45-49	M	NHB	c.76987G>A	p.Asp25663Asn	rs143186270	0.000105	326	A-band	100	0.49396
28	80-84	F	NHB	c.8938G>A	p.Ala2980Thr	rs72647885	0.000371	38	I-band	100	0.75822
29	70-74	F	NHB	c.9077A>T	p.Asn3026Ile	rs11900987	0.000454	38	I-band	100	0.56024
30	85-89	F	HL	c.7180G>C	p.Glu2394Gln	rs537269762	0.000004	31	I-band	100	0.58254
31	45-49	M	HL	c.57586C>G	p.Leu19196Val	rs397517630	0.000171	295	A-band	100	0.50185
32	60-64	F	NHB	c.44072C>T	p.Thr14691Ile	rs1048028645			I-band	100	0.73445
33	60-64	F	NHB	c.63245C>A	p.Thr21082Asn				A-band	100	0.74377
34	65-69	F	NHB	c.101936C>G	p.Pro33979Arg	rs200238877	0.000213	358	A-band	100	0.73517
35	65-69	F	NHB	c.57683G>A	p.Arg19228His	rs114711705	0.000488	295	A-band	100	0.30369
36	65-69	F	NHB	c.85691A>T	p.Lys28564Ile	rs199859344	0.000443	326	A-band	100	0.69443
37	55-59	M	NHB	c.44525C>T	p.Thr14842Ile	rs370782364	0.000012	241	I-band	100	0.75347
38	55-59	M	NHB	c.81502C>T	p.Arg27168Cys	rs377616334	0.000028	326	A-band	100	0.63269
39	65-69	F	NHB	c.88340C>G	p.Thr29447Arg	rs140201636	0.000198	331	A-band	100	0.58883
40	65-69	F	NHB	c.87137T>G	p.Met29046Arg	rs143975327	0.000192	328	A-band	100	0.81427
41	65-69	F	NHB	c.73316C>T	p.Thr24439Ile	rs750110781	0.000008	326	A-band	100	0.32913
42	60-64	F	NHB	c.98267C>T	p.Thr32756Ile	rs199805060	0.000330	352	A-band	100	0.58758
43	60-64	M	HL	c.91573A>G	p.Ile30525Val	rs72648244	0.006222	337	A-band	100	0.18881
44	60-64	M	HL	c.72931A>G	p.Thr24311Ala	rs56201325	0.003985	326	A-band	100	0.1533

Subject ID	Age	Sex	Race-Ethnicity	Nucleotide	Amino Acid Change	dbSNP	gnomAD Allele Frequency	Exon	Band	Percent Spliced In (PSI)	REVEL Score
45	60-64	F	NHB	c.8938G>A	p.Ala2980Thr	rs72647885	0.000371	38	I-band	100	0.75822
46	65-69	M	NHB	c.79612A>G	p.Thr26538Ala	rs150682764	0.000322	326	A-band	100	0.70029
47	65-69	M	HL	c.14911T>G	p.Cys4971Gly	rs537312655	0.000439	50	I-band	100	0.3358
48	55-59	M	NHB	c.43622C>T	p.Ser14541Leu	rs768180052	0.000008	236	I-band	100	0.60219
49	40-44	F	NHB	c.69883G>A	p.Ala23295Thr	rs746519147	0.000032	326	A-band	100	0.21907
50	75-79	M	NHB	c.52927C>T	p.Arg17643Trp	rs375944265	0.000060	276	A-band	100	0.75279
51	75-79	M	NHB	c.103363C>T	p.Arg34455Cys	rs72629785	0.000716	358	A-band	100	0.75687
52	75-79	M	NHB	c.81539T>C	p.Ile27180Thr	rs182126530	0.000669	326	A-band	100	0.64318
53	75-79	M	NHB	c.44077C>T	p.Arg14693Cys	rs200445568	0.000169	238	I-band	100	0.68844
54	60-64	M	NHB	c.103363C>T	p.Arg34455Cys	rs72629785	0.000716	358	A-band	100	0.75687
55	75-79	M	NHB	c.61481T>C	p.Ile20494Thr	rs374845737	0.000022	304	A-band	100	0.7293
56	50-54	F	NHB	c.54348A>T	p.Glu18116Asp	rs773746281	0.000016	281	A-band	100	0.48268
57	70-74	M	NHB	c.103906C>T	p.Arg34636Cys	rs768575577	0.000028	358	A-band	100	0.59861
58	70-74	M	NHB	c.97892A>T	p.Lys32631Ile	rs944963846	0.000004	351	A-band	100	0.56959
59	50-54	F	NHB	c.2765G>A	p.Arg922His	rs56046320	0.000703	16	near Z-disk	99	0.27141
60	50-54	F	NHB	c.60104G>A	p.Cys20035Tyr	rs774488793			A-band	100	0.71869
61	50-54	F	NHB	c.55079C>T	p.Pro18360Leu	rs192788942	0.000117	283	A-band	100	0.76881
62	90-94	M	HL	c.95414T>G	p.Phe31805Cys				A-band	100	0.73005
63	90-94	M	HL	c.74504A>G	p.Tyr24835Cys	rs201724962	0.000069	326	A-band	100	0.80901
64	55-59	M	NHB	c.78896T>A	p.Val26299Asp	rs73036377	0.000131	326	A-band	100	0.84613
65	45-49	M	NHB	c.101245G>A	p.Val33749Met	rs201554140	0.000538	358	A-band	100	0.72631
66	45-49	M	NHB	c.4199G>C	p.Ser1400Thr	rs138506461	0.000518	24	near Z-disk	100	0.12618
67	45-49	M	NHB	c.105127C>T	p.Arg35043Cys	rs200378865	0.000462	358	A-band	100	0.79765
68	50-54	M	NHB	c.2599A>G	p.Ser867Gly	rs148631577	0.000084	16	near Z-disk	99	0.27398
69	50-54	M	NHB	c.970C>T	p.Pro324Ser	rs72647845	0.000598	7	Z-disk	100	0.70603
70	55-59	F	NHB	c.69130C>T	p.Pro23044Ser	rs55980498	0.003619	324	A-band	100	0.83802
71	55-59	M	HL	c.95557C>A	p.Arg31853Ser				A-band	100	0.47777
72	55-59	M	HL	c.67989A>T	p.Leu22663Phe	rs1485610846	0.000004	320	A-band	100	0.71401
73	45-49	M	HL	c.88394C>T	p.Ser29465Phe	rs146181116	0.002928	331	A-band	100	0.65325
74	45-49	M	HL	c.89314G>A	p.Glu29772Lys	rs200503016	0.000245	334	A-band	100	0.5787
75	60-64	M	NHB	c.47737C>T	p.Leu15913Phe	rs138576504	0.000399	254	A-band	100	0.60456
76	60-64	M	NHB	c.98893G>A	p.Asp32965Asn	rs186405108	0.000044	353	A-band	100	0.68757
77	70-74	M	HL	c.93392T>G	p.Val31131Gly	rs1176407616	0.000012	339	A-band	100	0.47942
78	40-44	F	NHB	c.97760G>A	p.Arg32587His	rs55704830	0.001734	350	A-band	100	0.50341
79	55-59	F	NHB	c.95876T>A	p.Val31959Glu	rs761732372	0.000008	345	A-band	100	0.70924
80	95-99	F	HL	c.83870G>C	p.Arg27957Thr	rs148067743	0.000145	326	A-band	100	0.23913
81	50-54	F	NHB	c.61322A>G	p.Asn20441Ser	rs147580753	0.000260	304	A-band	100	0.34673
82	50-54	F	NHB	c.8938G>A	p.Ala2980Thr	rs72647885	0.000371	38	I-band	100	0.75822
83	70-74	F	HL	c.102030T>G	p.Ser34010Arg	rs1296387134	0.000024	358	A-band	100	0.69273
84	60-64	F	HL	c.102427A>T	p.Met34143Leu	rs371226574	0.000004	358	A-band	100	0.46781
85	60-64	F	HL	c.96928A>C	p.Thr32310Pro	rs542208825	0.000024	348	A-band	100	0.46444
86	60-64	F	HL	c.56315C>T	p.Thr18772Ile	rs370118111	0.000008	289	A-band	100	0.57482
87	60-64	M	NHB	c.9077A>T	p.Asn3026Ile	rs11900987	0.000454	38	I-band	100	0.56024
88	60-64	M	NHB	c.82411G>A	p.Gly27471Ser	rs757130634			A-band	100	0.31778
89	70-74	M	NHB	c.98893G>C	p.Asp32965His	rs186405108	0.000213	353	A-band	100	0.70276

Subject ID	Age	Sex	Race-Ethnicity	Nucleotide	Amino Acid Change	dbSNP	gnomAD Allele Frequency	Exon	Band	Percent Spliced In (PSI)	REVEL Score
90	70-74	M	NHB	c.72137C>T	p.Ala24046Val	rs146767076	0.000363	326	A-band	100	0.20419
91	70-74	M	NHB	c.72782G>A	p.Arg24261Gln	rs142874389	0.000574	326	A-band	100	0.65522
92	70-74	M	NHB	c.55951G>A	p.Glu18651Lys				A-band	100	0.6251
93	70-74	M	NHB	c.44965A>G	p.Ile14989Val	rs755040094	0.000004	244	I-band	100	0.50496
94	70-74	M	NHB	c.88973T>C	p.Ile29658Thr	rs750026544	0.000024	333	A-band	100	0.16972
95	60-64	M	NHB	c.106439A>G	p.His35480Arg	rs766337455			M-band	100	0.25558
96	55-59	F	NHB	c.69383C>A	p.Ser23128Tyr	rs72646882	0.000576	324	A-band	100	0.76554
97	75-79	F	NHB	c.47770T>A	p.Leu15924Met				A-band	100	0.83636
98	25-29	M	HL	c.64997C>T	p.Ala21666Val	rs1396380194	0.000004	311	A-band	100	0.5065
99	25-29	M	HL	c.106349C>G	p.Thr35450Ser	rs371022420	0.000045	358	A-band	100	0.30369
100	25-29	M	HL	c.97760G>C	p.Arg32587Pro	rs55704830	0.000393	350	A-band	100	0.58633
101	25-29	M	HL	c.57165A>T	p.Glu19055Asp	rs1263660973	0.000004	293	A-band	100	0.58507
102	25-29	M	HL	c.73168A>G	p.Thr24390Ala	rs182491843	0.000481	326	A-band	100	0.08068
103	25-29	M	HL	c.76141G>A	p.Ala25381Thr	rs763636099	0.000008	326	A-band	100	0.84345
104	25-29	M	HL	c.106827T>G	p.Ile35609Met	rs727504540	0.000337	360	M-band	100	0.53062
105	50-54	F	HL	c.88394C>T	p.Ser29465Phe	rs146181116	0.002928	331	A-band	100	0.65325
106	60-64	F	NHB	c.79612A>G	p.Thr26538Ala	rs150682764	0.000322	326	A-band	100	0.70029
107	65-69	M	HL	c.84309C>G	p.His28103Gln	rs749278779	0.000004	326	A-band	100	0.35528
108	60-64	M	NHB	c.44077C>T	p.Arg14693Cys	rs200445568	0.000169	238	I-band	100	0.68844
109	60-64	M	NHB	c.6927T>A	p.Asn2309Lys	rs147580120	0.000024	30	I-band	100	0.2335
110	60-64	M	NHB	c.81539T>C	p.Ile27180Thr	rs182126530	0.000669	326	A-band	100	0.64318
111	65-69	M	NHB	c.47737C>T	p.Leu15913Phe	rs138576504	0.000399	254	A-band	100	0.60456
112	65-69	M	NHB	c.55547T>C	p.Ile18516Thr	rs146608896	0.000467	287	A-band	100	0.78662
113	60-64	M	NHB	c.87611C>G	p.Thr29204Arg	rs72648228	0.000157	328	A-band	100	0.29647
114	60-64	M	NHB	c.2764C>T	p.Arg922Cys	rs72647862	0.000331	16	near Z-disk	99	0.54641
115	60-64	M	NHB	c.86393G>A	p.Arg28798Lys	rs781458689	0.000008	326	A-band	100	0.62838
116	60-64	M	NHB	c.62432A>G	p.Asp20811Gly	rs72646849	0.000165	304	A-band	100	0.76487
117	70-74	F	HL	c.57145G>A	p.Val19049Ile	rs750251277	0.000080	293	A-band	100	0.56694
118	70-74	F	HL	c.92444G>A	p.Cys30815Tyr	rs1185347998	0.000004	339	A-band	100	0.59375
119	80-84	M	HL	c.8509A>G	p.Ser2837Gly	rs202024134	0.000004	36	I-band	100	0.43662
120	80-84	M	HL	c.86759C>G	p.Ser28920Cys	rs1396089552	0.000004	326	A-band	100	0.36365
121	80-84	M	HL	c.92176C>T	p.Pro30726Ser	rs72648247	0.002682	339	A-band	100	0.79583
122	75-79	M	NHB	c.101245G>A	p.Val33749Met	rs201554140	0.000538	358	A-band	100	0.72631
123	75-79	M	NHB	c.4199G>C	p.Ser1400Thr	rs138506461	0.000518	24	near Z-disk	100	0.12618
124	75-79	M	NHB	c.105127C>T	p.Arg35043Cys	rs200378865	0.000462	358	A-band	100	0.79765
125	45-49	F	NHB	c.46040T>G	p.Val15347Gly	rs375367475	0.000044	248	I-band	100	0.77783
126	45-49	F	NHB	c.72782G>A	p.Arg24261Gln	rs142874389	0.000574	326	A-band	100	0.65522
127	45-49	F	NHB	c.72137C>T	p.Ala24046Val	rs146767076	0.000363	326	A-band	100	0.20419
128	65-69	F	NHB	c.97106C>T	p.Thr32369Ile	rs559194338	0.000004	348	A-band	100	0.62729
129	75-79	F	NHB	c.50390G>A	p.Arg16797His	rs200835354	0.000093	268	A-band	100	0.71084
130	65-69	F	HL	c.94851T>A	p.Asp31617Glu	rs72648256	0.002881	342	A-band	100	0.6823
131	65-69	F	HL	c.14870C>G	p.Thr4957Ser	rs72648925	0.002917	50	I-band	100	0.28911
132	65-69	M	NHB	c.101936C>G	p.Pro33979Arg	rs200238877	0.000213	358	A-band	100	0.73517
133	65-69	M	NHB	c.85691A>T	p.Lys28564Ile	rs199859344	0.000443	326	A-band	100	0.69443
134	65-69	M	NHB	c.57683G>A	p.Arg19228His	rs114711705	0.000488	295	A-band	100	0.30369

Subject ID	Age	Sex	Race-Ethnicity	Nucleotide	Amino Acid Change	dbSNP	gnomAD Allele Frequency	Exon	Band	Percent Spliced In (PSI)	REVEL Score
135	65-69	F	NHB	c.61138C>A	p.Leu20380Met	rs201167216	0.000271	304	A-band	100	0.41658
136	65-69	F	NHB	c.86911G>A	p.Gly28971Arg	rs368921501	0.000040	327	A-band	100	0.79217
137	65-69	F	NHB	c.66692G>A	p.Arg22231His	rs200971254	0.000343	316	A-band	100	0.76881
138	65-69	F	HL	c.69130C>T	p.Pro23044Ser	rs55980498	0.003619	324	A-band	100	0.83802

Supplementary Table 1: List of *TTN* missense variants. Age represents patient's age at AF diagnosis in years. M=male, F=female, HL = Hispanic/Latinx, NHB = non-Hispanic Black. Variants with a blank value in the dbSNP or gnomAD columns represent variants not present in those respective databases.

	Predicted Deleterious *TTN* Missense Absent (N=88)	Predicted Deleterious *TTN* Missense Present (N=43)	Total (N=131)	P-value
Age at AF diagnosis (years)	63.7 (14.5)	63.0 (12.5)	63.5 (13.8)	0.803
Male sex	47 (53.4%)	23 (53.5%)	70 (53.4%)	1.000
Race/ethnicity				0.026
Non-Hispanic Black	57 (64.8%)	36 (83.7%)	93 (71.0%)	
Hispanic/Latinx	31 (35.2%)	7 (16.3%)	38 (29.0%)	
BMI (kg/m^2)	33.8 (8.9)	34.9 (11.1)	34.1 (9.7)	0.540
Diabetes	35 (39.8%)	15 (34.9%)	50 (38.2%)	0.702
Hypertension	77 (87.5%)	36 (83.7%)	113 (86.3%)	0.594
Coronary artery disease	19 (21.6%)	13 (30.2%)	32 (24.4%)	0.288
History of stroke/transient ischemic attack	17 (19.3%)	9 (20.9%)	26 (19.8%)	0.819
Congestive heart failure	32 (36.4%)	22 (51.2%)	54 (41.2%)	0.131
Nonischemic dilated cardiomyopathy	6 (7.1%)	6 (15.4%)	12 (9.7%)	0.191
Estimated glomerular filtration rate (mg/dL)	69.1 (24.6)	68.9 (24.8)	69.1 (24.6)	0.965
Ventricular rate	90.9 (27.4)	103.7 (31.4)	95.3 (29.4)	0.022
QRS interval (ms)	97.3 (24.3)	102.7 (30.0)	99.2 (26.3)	0.292
QTc interval (ms)	453.9 (38.7)	470.6 (44.0)	459.6 (41.2)	0.035
Left ventricular ejection fraction (%)				0.144
Normal (>/=50%)	55 (62.5%)	22 (51.2%)	77 (58.8%)	
Mildly decreased (40-49%)	11 (12.5%)	3 (7.0%)	14 (10.7%)	
Moderately decreased (30-39%)	7 (8.0%)	6 (14.0%)	13 (9.9%)	
Severely decreased (20-29%)	8 (9.1%)	8 (18.6%)	16 (12.2%)	
Very severely decreased (< 20%)	7 (8.0%)	4 (9.3%)	11 (8.4%)	
Left ventricular end diastolic diameter (mm)	45.6 (9.2)	49.8 (8.0)	46.9 (9.0)	0.021
Left ventricular dilatation	9 (11.8%)	8 (22.2%)	17 (15.2%)	0.168
Left atrial size				0.728
Normal	26 (31.3%)	12 (28.6%)	38 (30.4%)	
Mildly dilated	22 (26.5%)	16 (38.1%)	38 (30.4%)	
Moderately dilated	22 (26.5%)	8 (19.0%)	30 (24.0%)	
Severely dilated	13 (15.7%)	6 (14.3%)	19 (15.2%)	
Left atrial diameter (mm)	39.8 (7.5)	41.5 (8.4)	40.4 (7.8)	0.293

Supplementary Table 2: Clinical characteristics of ethnic minority subjects with AF stratified by presence of predicted deleterious rare missense *TTN* variants. *Data are missing for the following variables: eGFR (1), electrocardiogram within 3 months of AF diagnosis (11), LVEDD (19), left atrial size (6), left atrial diameter (21). Left ventricular dilatation is defined as left ventricular end diastolic diameter greater than 2 standard deviations above the normal sex-specific mean value. Variants with a REVEL score ≥ 0.7 were defined as predicted deleterious. Continuous data are

represented as mean (standard deviation) and categorical data are represented as count (%).

Subject ID	Age	Sex	Race-Ethnicity	Nucleotide	Amino Acid Change	Exon	Band	Percent Spliced In (PSI)	REVEL Score	LVEDD (mm)	LVEF (%)
1	55-59	F	NHB	c.70250T>C	p.Ile23417Thr	326	A-band	100	0.66297	57.9	Mildly decreased (40-49%)
2	40-44	F	NHB	c.101665G>A	p.Val33889Ile	358	A-band	100	0.17295	53.2	Mildly decreased (40-49%)
3	40-44	F	NHB	c.6959G>A	p.Arg2320His	30	I-band	100	0.82403	53.2	Mildly decreased (40-49%)
4	65-69	F	NHB	c.91937A>G	p.Asn30646Ser	338	A-band	100	0.71558	56.9	Severely decreased (20-29%)
5	65-69	F	NHB	c.46693G>T	p.Ala15565Ser	250	I-band	100	0.51417	56.9	Severely decreased (20-29%)
6	55-59	M	NHB	c.44525C>T	p.Thr14842Ile	241	I-band	100	0.75347	59.0	Very severely decreased (< 20%)
7	55-59	M	NHB	c.81502C>T	p.Arg27168Cys	326	A-band	100	0.63269	59.0	Very severely decreased (< 20%)
8	40-44	F	NHB	c.69883G>A	p.Ala23295Thr	326	A-band	100	0.21907	60.3	Moderately decreased (30-39%)
9	45-49	M	NHB	c.101245G>A	p.Val33749Met	358	A-band	100	0.72631	66.5	Very severely decreased (< 20%)
10	45-49	M	NHB	c.4199G>C	p.Ser1400Thr	24	near Z-disk	100	0.12618	66.5	Very severely decreased (< 20%)
11	45-49	M	NHB	c.105127C>T	p.Arg35043Cys	358	A-band	100	0.79765	66.5	Very severely decreased (< 20%)
12	25-29	M	HL	c.64997C>T	p.Ala21666Val	311	A-band	100	0.5065	60.3	Severely decreased (20-29%)
13	25-29	M	HL	c.106349C>G	p.Thr35450Ser	358	A-band	100	0.30369	60.3	Severely decreased (20-29%)
14	25-29	M	HL	c.97760G>C	p.Arg32587Pro	350	A-band	100	0.58633	60.3	Severely decreased (20-29%)
15	25-29	M	HL	c.57165A>T	p.Glu19055Asp	293	A-band	100	0.58507	60.3	Severely decreased (20-29%)
16	25-29	M	HL	c.73168A>G	p.Thr24390Ala	326	A-band	100	0.08068	60.3	Severely decreased (20-29%)
17	25-29	M	HL	c.76141G>A	p.Ala25381Thr	326	A-band	100	0.84345	60.3	Severely decreased (20-29%)
18	25-29	M	HL	c.106827T>G	p.Ile35609Met	360	M-band	100	0.53062	60.3	Severely decreased (20-29%)
19	65-69	M	NHB	c.47737C>T	p.Leu15913Phe	254	A-band	100	0.60456	66.2	Moderately decreased (30-39%)
20	65-69	M	NHB	c.55547T>C	p.Ile18516Thr	287	A-band	100	0.78662	66.2	Moderately decreased (30-39%)

Supplementary Table 3: *TTN* missense variants in subjects meeting criteria for nonischemic dilated cardiomyopathy. Nonischemic dilated cardiomyopathy was defined by left ventricular ejection fraction <50% and left ventricular end diastolic diameter (LVEDD) greater than 2 standard deviations above the sex-specific mean, as well as coronary angiogram confirming the absence of obstructive coronary artery disease.

	Unadjusted			Partially Adjusted			Fully Adjusted		
Characteristic	**HR[1]**	**95% CI[1]**	**p-value**	**HR[1]**	**95% CI[1]**	**p-value**	**HR[1]**	**95% CI[1]**	**p-value**
TTN Missense Present	1.81	1.04, 3.15	0.036	1.82	1.04, 3.17	0.035	1.80	1.03, 3.15	0.039
Age (years)				0.99	0.97, 1.01	0.366	0.99	0.97, 1.01	0.430
Male sex (vs. female)				0.74	0.43, 1.27	0.268	0.69	0.38, 1.24	0.218
Race-ethnicity									
Non-Hispanic Black							—	—	
Hispanic/Latinx							1.14	0.60, 2.19	0.683
Baseline ejection fraction <50%							1.38	0.78, 2.44	0.272

[1]HR = Hazard Ratio, CI = Confidence Interval

Supplementary Table 4: Parameter estimates for univariable and multivariable Cox proportional hazard models of atrial fibrillation and heart failure-related hospitalizations. A partially adjusted multivariable model contained covariates of age and sex, and the fully adjusted model additionally accounted for race-ethnicity and ejection fraction <50% closest to AF diagnosis.

	Unadjusted			Partially Adjusted			Fully Adjusted		
Characteristic	**HR[1]**	**95% CI[1]**	**p-value**	**HR[1]**	**95% CI[1]**	**p-value**	**HR[1]**	**95% CI[1]**	**p-value**
TTN Missense									
None	—	—		—	—		—	—	
REVEL <0.70	1.60	0.78, 3.28	0.198	1.61	0.79, 3.26	0.188	1.60	0.80, 3.21	0.182
REVEL ≥0.70	1.92	1.04, 3.53	0.036	1.92	1.04, 3.56	0.038	1.91	1.04, 3.51	0.038
Age (years)				0.99	0.97, 1.01	0.363	0.99	0.97, 1.01	0.412
Male sex (vs. female)				0.73	0.42, 1.25	0.251	0.68	0.38, 1.23	0.204
Race-ethnicity									
Non-Hispanic Black							—	—	
Hispanic/Latinx							1.17	0.63, 2.16	0.619
Baseline ejection fraction <50%							1.35	0.77, 2.36	0.302

[1]HR = Hazard Ratio, CI = Confidence Interval

Supplementary Table 5: Cox proportional hazard models of hospitalizations related to TTN missense variants based on *in silico* prediction of impact. REVEL score of ≥0.70 indicates potentially deleterious effect. A partially adjusted multivariable model contained covariates of age and sex, and the fully adjusted model additionally accounted for race-ethnicity and ejection fraction <50% closest to AF diagnosis.

	Unadjusted			Partially Adjusted			Fully Adjusted		
Characteristic	**HR[1]**	**95% CI[1]**	**p-value**	**HR[1]**	**95% CI[1]**	**p-value**	**HR[1]**	**95% CI[1]**	**p-value**
TTN Missense Present	1.81	1.00, 3.29	0.051	1.84	1.01, 3.34	0.046	1.83	1.01, 3.32	0.046
Age (years)				0.99	0.97, 1.01	0.365	0.99	0.97, 1.01	0.360
Male sex (vs. female)				0.75	0.42, 1.35	0.344	0.70	0.37, 1.32	0.268
Race-ethnicity									
Non-Hispanic Black							—	—	
Hispanic/Latinx							1.17	0.59, 2.31	0.649
Baseline ejection fraction <50%							1.41	0.76, 2.61	0.280

[1]HR = Hazard Ratio, CI = Confidence Interval

Supplementary Table 6: Cox proportional hazard models of hospitalizations excluding cases with nonischemic dilated cardiomyopathy. A total of 12 subjects were excluded. A partially adjusted multivariable model contained covariates of age and sex, and the fully adjusted model additionally accounted for race-ethnicity and ejection fraction <50% closest to AF diagnosis.

Nucleotide and Protein ID	NM_001267550.2(TTN):c.98267C>T (NP_001254479.2:p.Thr32756Ile)
Allele ID	173049
Variant type	single nucleotide variant (missense)
Variant length	1 bp
Cytogenetic location	2q31.2
Genomic location	2: 178539798 (GRCh38) GRCh38 UCSC; 2: 179404525 (GRCh37) GRCh37 UCSC
Canonical SPDI	NC_000002.12:178539797:G:A
Source	https://www.ncbi.nlm.nih.gov/clinvar/variation/178164/

Supplementary Table 7: *TTN*-T32756I variant information.

ACKNOWLEDGEMENT

This work was in part supported by NIH grants R01 HL150586 (DD), R01 HL148444 (DD), NIH T32 HL139439 and AHA 23POST1019044 (MH), UL1 TR002003 (The University of Illinois Chicago Center for Clinical and Translational Science (CCTS)), AHA CDA (MAP), and UIC seed funding (MAP).

CONTRIBUTIONS

DD and MAP conceived the project, designed the experiments, analyzed the data, and wrote the manuscript. MAP and JD performed electrophysiological experiments. HC carried out cell culture, generated atrial and mutated iPSC lines. MCH analyzed the clinical data with the help of SS, generated the clinical figures and table, and wrote the clinical sections of the results, methods, and discussion. FD, AOL, BAA, and BC assisted with obtaining the clinical data. MAP, HC, AS, MB, and AO performed contractility, optical voltage mapping, calcium handling, qPCR, western blotting, RNA-seq, and other molecular analyses. JR helped interpreting the RNA-sequencing data and iPSC differentiation approaches. All authors revised the manuscript.

COMPETING INTERESTS

The authors declare no competing interests.

MATERIALS & CORRESPONDENCE

gmmahmud@uic.edu, darbar@uic.edu